J. Fluid Mech. (2019), *vol.* 871, *pp.* 244–270. © Cambridge University Press 2019
doi:10.1017/jfm.2019.337

Multiscale preferential sweeping of particles settling in turbulence

Josin Tom[1] **and Andrew D. Bragg**[1,†]

[1]Department of Civil and Environmental Engineering, Duke University, Durham, NC 27708, USA

(Received 20 December 2018; revised 19 March 2019; accepted 21 April 2019;
first published online 20 May 2019)

In a seminal article, Maxey (*J. Fluid Mech.*, vol. 174, 1987, pp. 441–465) presented a theoretical analysis showing that enhanced particle settling speeds in turbulence occur through the preferential sweeping mechanism, which depends on the preferential sampling of the fluid velocity gradient field by the inertial particles. However, recent direct numerical simulation (DNS) results in Ireland *et al.* (*J. Fluid Mech.*, vol. 796, 2016*b*, pp. 659–711) show that even in a portion of the parameter space where this preferential sampling is absent, the particles nevertheless exhibit enhanced settling velocities. Further, there are several outstanding questions concerning the role of different turbulent flow scales on the enhanced settling, and the role of the Taylor Reynolds number R_λ. The analysis of Maxey does not explain these issues, partly since it was restricted to particle Stokes numbers $St \ll 1$. To address these issues, we have developed a new theoretical result, valid for arbitrary St, that reveals the multiscale nature of the mechanism generating the enhanced settling speeds. In particular, it shows how the range of scales at which the preferential sweeping mechanism operates depends on St. This analysis is complemented by results from DNS where we examine the role of different flow scales on the particle settling speeds by coarse graining the underlying flow. The results show how the flow scales that contribute to the enhanced settling depend on St, and that contrary to previous claims, there can be no single turbulent velocity scale that characterizes the enhanced settling speed. The results explain the dependence of the particle settling speeds on R_λ, and show how the saturation of this dependence at sufficiently large R_λ depends upon St. The results also show that as the Stokes settling velocity of the particles is increased, the flow scales of the turbulence responsible for enhancing the particle settling speed become larger. Finally, we explored the multiscale nature of the preferential sweeping mechanism by considering how particles preferentially sample the fluid velocity gradients coarse grained at various scales. The results show that while rapidly settling particles do not preferentially sample the fluid velocity gradients, they do preferentially sample the fluid velocity gradients coarse grained at scales outside of the dissipation range. This explains the findings of Ireland *et al.*, and further illustrates the truly multiscale nature of the mechanism generating enhanced particle settling speeds in turbulence.

Key words: isotropic turbulence, multiphase flow, particle/fluid flow

† Email address for correspondence: andrew.bragg@duke.edu

https://doi.org/10.1017/jfm.2019.337 Published online by Cambridge University Press

1. Introduction

The motion of inertial particles in turbulence settling under gravity is important for many environmental, biological and engineering multiphase flows such as water droplets in clouds (Shaw 2003; Grabowski & Wang 2013), marine snow (Kiorboe 1997; Guseva *et al.* 2016) and sediment transport (Papanicolaou *et al.* 2008). For these problems, it is important to quantify the settling speed of the particles as they fall through the turbulent flow, since this determines the vertical mass flux of the particles. In a still fluid of infinite extent, small particles settle with the Stokes settling velocity (Batchelor 1967), which is determined by the balance of drag and gravity forces acting on the particles. In a turbulent flow, the drag forces acting on the particles fluctuate, and an important question is whether these fluctuations modify the average settling velocity of the particles compared with that in a still fluid.

The answer to this question depends upon the parameters of the system. For the case of small (diameter much smaller than the Kolmogorov length scale η), and heavy (particle density much greater than fluid density) inertial particles, two important parameters are the particle Stokes number, St, and the Froude number, Fr. The Stokes number, $St \equiv \tau_p/\tau_\eta$, provides a measure of the particle inertia, where τ_p is the particle response time and τ_η is the Kolmogorov time scale. The Froude number, $Fr \equiv a_\eta/g$, quantifies the strength of the turbulence relative to gravity, where a_η is the Kolmogorov acceleration scale and g is the magnitude of the gravitational acceleration. From St and Fr the settling parameter can be defined $Sv \equiv St/Fr \equiv \tau_p g/u_\eta$, that compares the Stokes settling velocity to the Kolmogorov velocity scale u_η. Another important parameter is the particle Reynolds number, Re_p, that determines whether the drag force on the particle is a linear or nonlinear function of the slip velocity between the particle and local fluid velocity (Maxey & Riley 1983). It is typically assumed that the drag force is linear if $Re_p < 0.5$ (Elghobashi & Truesdell 1993).

For particles subject to a linear drag force, Reeks (1977) argued that in a stochastic random fluid velocity field, there would be no net effect of the flow fluctuations on the average particle settling velocity. In contrast, Maxey & Corrsin (1986) performed a numerical study and demonstrated that aerosol particles subject to a linear drag force settle more rapidly in a randomly oriented, periodic, cellular flow field than they do in a still fluid. In a seminal article, Maxey (1987) reported enhanced particle settling velocities in simulations using a linear drag force and a Gaussian fluid velocity field. He then presented a detailed theoretical analysis for $St \ll 1$ to show that enhanced particle settling speeds in spatio-temporally correlated fluid velocity fields can occur because inertial particles preferentially sample low vorticity regions of the fluid velocity field where the flow is moving down (in the direction of gravity). Maxey argued that this preferential sampling occurs because inertial particles are centrifuged out of regions of strong vorticity, something that was subsequently confirmed by Squires & Eaton (1991) using direct numerical simulations (DNS) of particle motion in turbulence. In a subsequent work, Wang & Maxey (1993) performed DNS for small, heavy settling particles subject to linear drag, and observed significant enhancement of the particle settling velocities due to turbulence for particles with $Sv = O(1)$ and $St = O(1)$. They also confirmed the physical argument of Maxey (1987) that settling inertial particles preferentially accumulate in low vorticity regions of the flow where fluid velocity aligns with the direction of gravity. They referred to this effect as the 'preferential sweeping mechanism' or 'fast tracking', and it has since been observed in several DNS (Bec, Homann & Ray 2014; Rosa *et al.* 2016; Ireland, Bragg & Collins 2016*b*; Monchaux & Dejoan 2017) and experimental studies (Aliseda *et al.* 2002; Good *et al.* 2014; Petersen, Baker & Coletti 2019).

https://doi.org/10.1017/jfm.2019.337 Published online by Cambridge University Press

When $Re_p > 1$, a nonlinear drag law should be used for calculating the drag force on the particle (Clift, Grace & Weber 1978). Early experimental works (Tunstall & Houghton 1968; Schneborn 1975) have shown that the combination of particle inertia and nonlinear drag can reduce the settling velocity in simple oscillatory flows. Two common ways of introducing nonlinear drag are to use a simple square drag law (Fung 1993), or use an empirical relationship for the drag coefficient based on the instantaneous particle Reynolds number (Fung 1998). Fung (1993) used a simple Gaussian fluid velocity field with a square drag law, and observed a decrease of the particle settling velocities compared with the linear drag case, as did Mei (1994) who prescribed the fluid velocity using a stochastic process and employed a nonlinear drag coefficient. In contrast, Chan & Fung (1999) found an increase in the particle settling velocity due to nonlinear drag for particles settling in a simple, two-dimensional periodic cellular flow with a square drag law. Nielsen (1984) used an analytical solution approach to argue that the reduction in the particle settling velocity due to nonlinear drag is negligible.

These studies on the effects of nonlinear drag on particle settling speeds did not, however, consider real turbulence, but only simple random flow fields. Nevertheless, DNS studies have also come to conflicting conclusions concerning the role of nonlinear drag on particle settling speeds in turbulence. Wang & Maxey (1993) studied the influence of a nonlinear drag coefficient using DNS and found that its effect was to only slightly reduce the particle settling speeds compared to the linear drag case, with similar results in Rosa *et al.* (2016). However, Good *et al.* (2014) observed a significant reduction in the particle settling velocity compared with the linear drag case, in certain regimes of St, Sv.

Another issue is whether in some cases it is possible for turbulence to reduce the particle settling speed compared with the Stokes settling velocity. This scenario, referred to by Nielsen (1993) as 'loitering', could occur when the particles spend more time in upward moving regions of the flow than downward moving regions. In their DNS study using nonlinear drag, Wang & Maxey (1993) observed loitering only in a limited portion of the parameter space. Loitering has been observed in several experiments (Yang & Shy 2003; Kawanisi & Shiozaki 2008; Good *et al.* 2014), while the recent detailed measurements of Petersen *et al.* (2019) did not show clear evidence of loitering. Good *et al.* (2014) were only able to observe loitering in their DNS when either the horizontal motion of the particles was artificially eliminated, or else when a nonlinear drag force was used for the particles. However, as discussed earlier, other studies such as Rosa *et al.* (2016) have found only a small effect of nonlinear drag on the particle settling speeds, and they did not observe loitering.

These studies show that even for the relatively simple case of small particles settling in turbulence, the role of turbulence on the average particle settling speed is subtle, and a number of issues remain to be solved. Moreover, there are other additional complexities that can modify particle settling speeds in turbulence, including finite particle size effects (Fornari *et al.* 2016), particle–fluid two-way coupling (Monchaux & Dejoan 2017) and collective particle interaction effects (Huck *et al.* 2018), all of which significantly complicate the problem.

Even in the absence of these additional complexities, an aspect of the problem that has not been systematically explored concerns the role of different turbulent flow scales in modifying the particle settling speeds in turbulence. Due in part to its restriction to $St \ll 1$, the theoretical analysis of Maxey (1987) gives little insight into which scales of the turbulence contribute to the particle settling speeds. Numerical studies, have, to a limited extent, considered the question of which flow scales

https://doi.org/10.1017/jfm.2019.337 Published online by Cambridge University Press

contribute to the enhanced settling. Wang & Maxey (1993) argued that their DNS results implied that the enhanced particle settling speeds due to turbulence depends on the fluid root-mean-square (r.m.s.) velocity u', which is associated with the large scales of the turbulent flow. However, they also argued that this could be an artefact of the low Reynolds number of their DNS, and that in real atmospheric flows where the scale separation is much larger, the particle settling speeds are likely to be only affected by a limited range of scales of the turbulence. The study of Yang & Lei (1998) considered the role played by different flow scales on the particle settling speeds in turbulence using DNS and large-eddy simulations (LES). They concluded that the large scales of the flow play a key role and that the relevant fluid velocity scale determining the settling enhancement is u' and not u_η. However, they also concluded that the settling enhancement depends on the particle inertia through τ_p/τ_η, and not τ_p/τ_L, where τ_L is the integral time scale of the flow. Their argument is that the preferential sweeping effect depends on the small scale clustering of the particles, and hence τ_η, while the drag force on the particles depends mainly on the large scales, and hence u'. The recent study of Rosa *et al.* (2016) also argued that the relevant fluid velocity scale determining the settling enhancement is u'.

The success of 'mixed scaling', i.e. using a large scale quantity u' for the velocity scale, and a small scale quantity τ_η for the time scale, used in previous studies (Yang & Lei 1998; Good *et al.* 2014), reveal something of the multiscale nature of the problem, and that both large and small scales of the turbulence affect the settling speeds. However, there is a need to elucidate whether the single velocity scale u' really does dominate the particle settling speeds, or whether there exists a range of velocity scales that govern the process. Indeed, as we shall point out in § 2, there are theoretical difficulties with the argument that the relevant turbulent velocity scale dominating the settling speed is u'. Moreover, it is not at all obvious that a single velocity scale should determine the settling speed, independent of St, since the interaction of an inertial particle with a given flow scale depends strongly on St. Motivated by the need to develop particle subgrid scale (SGS) models for LES of particles settling in turbulent flows, Rosa & Pozorski (2017) used numerical simulations to study the effect of the small scales of the turbulence on particle settling speeds. Their results showed that scales smaller than a certain size did not affect the particle settling speeds. However, they did not consider whether there exists an upper limit to the range of scales that affect the particle settling speeds, nor did they provide detailed information concerning how the range of velocity scales impacting the settling speeds might depend on St or Fr.

In addition to these open issues, results in Ireland *et al.* (2016*b*) showed that significant enhancement of particle settling speeds due to turbulence are observed for $St \geqslant O(1)$ and $Fr \ll 1$, even though the DNS data showed that for $St \geqslant O(1)$ and $Fr \ll 1$ the particles do not preferentially sample the fluid velocity gradient field. This seems inconsistent with the preferential sweeping mechanism which relies on the idea that inertial particles do preferentially sample the fluid velocity gradient field, showing a preference to avoid regions dominated by vorticity due to the centrifuge effect.

In order to resolve these issues and provide insight into the role of different flow scales on the enhanced settling speeds of particles in turbulence, it is desirable to develop a theoretical framework that goes beyond the work of Maxey (1987) that restricted attention to $St \ll 1$. The purpose of the present study then is to address these issues and provide insight concerning which flow scales contribute to the modified particle settling speeds due to turbulence. To this end, we develop a new

https://doi.org/10.1017/jfm.2019.337 Published online by Cambridge University Press

theoretical framework for analysing the problem for arbitrary St, which is then used in conjunction with DNS data for a range of Reynolds numbers to provide detailed insights into the multiscale mechanism leading to enhanced particle settling speeds in turbulence.

2. Theory

2.1. *Background*

We consider the settling of small ($d_p/\eta \ll 1$, where d_p is the particle diameter), heavy ($\rho_p/\rho_f \gg 1$, where ρ_p is particle density and ρ_f is fluid density), spherical inertial particles, that are one-way coupled to a statistically stationary isotropic turbulent flow. In the regime of a linear drag force on the particles, the particle equation of motion reduces to (see Maxey & Riley 1983)

$$\ddot{\boldsymbol{x}}^p(t) \equiv \dot{\boldsymbol{v}}^p(t) = \frac{1}{St\tau_\eta}(\boldsymbol{u}(\boldsymbol{x}^p(t), t) - \boldsymbol{v}^p(t)) + \boldsymbol{g}, \tag{2.1}$$

where $\boldsymbol{x}^p(t)$, $\boldsymbol{v}^p(t)$ are the particle position and velocity vectors, respectively, $\boldsymbol{u}(\boldsymbol{x}^p(t), t)$ is the fluid velocity at the particle position and $\boldsymbol{g}$ is the gravitational acceleration vector.

As discussed earlier, some studies suggest that for $Sv \geqslant O(10)$, nonlinear drag effects are important for settling particle motion in turbulence (Good *et al.* 2014), while other studies suggest that even up to $Sv \approx 63$, the effects of nonlinear drag are very small (Rosa *et al.* 2016). Such discrepancies must be resolved in future work. However, in the present study we will ignore nonlinear corrections to the drag force for analytical simplicity, leaving the consideration of nonlinear drag, as well as other complexities such as two-way momentum coupling with the fluid, for future work.

For the system described above, the ensemble average of (2.1) in the direction of gravity $\boldsymbol{e}_z$ gives

$$\langle v_z^p(t)\rangle = \langle u_z(\boldsymbol{x}^p(t), t)\rangle + St\tau_\eta g, \tag{2.2}$$

since $\langle \dot{\boldsymbol{v}}^p(t)\rangle = \boldsymbol{0}$ for this system. Equation (2.2) shows that the average particle velocity may differ from the Stokes settling velocity $St\tau_\eta g$ only if $\langle u_z(\boldsymbol{x}^p(t), t)\rangle \neq 0$. Numerous studies, both numerical (Wang & Maxey 1993; Bec *et al.* 2014; Rosa *et al.* 2016; Ireland *et al.* 2016*b*; Monchaux & Dejoan 2017) and experimental (Aliseda *et al.* 2002; Good *et al.* 2014; Petersen *et al.* 2019), have indeed shown that $\langle v_z^p(t)\rangle \neq St\tau_\eta g$, implying $\langle u_z(\boldsymbol{x}^p(t), t)\rangle \neq 0$. Maxey (1987) developed a theoretical framework to explain how $\langle u_z(\boldsymbol{x}^p(t), t)\rangle \neq 0$, even though the Eulerian average satisfies $\langle u_z(\boldsymbol{x}, t)\rangle = 0$ for an isotropic flow. Essentially, the explanation is that particles with inertia do not uniformly sample the underlying fluid velocity field, and that gravity leads to a bias for inertial particles to accumulate in regions of the flow where $\boldsymbol{e}_z \cdot \boldsymbol{u} > 0$. However, the analysis of Maxey (1987) is restricted to $St \ll 1$.

A key question concerns which scales of the turbulent flow influence the quantity $\langle u_z(\boldsymbol{x}^p(t), t)\rangle$. While this has not previously been systematically explored, one claim that has been made in numerous studies (Wang & Maxey 1993; Yang & Lei 1998; Good *et al.* 2014; Nemes *et al.* 2017; Petersen *et al.* 2019) is that $\langle u_z(\boldsymbol{x}^p(t), t)\rangle$ depends on u', the large scale fluid velocity. However, this seems unlikely because if $\langle u_z(\boldsymbol{x}^p(t), t)\rangle$ depends on u', then even if $Sv = O(1)$, $\langle u_z(\boldsymbol{x}^p(t), t)\rangle/u_\eta \to \infty$ as $R_\lambda \to \infty$ since $u'/u_\eta \sim R_\lambda^{1/2}$ (Pope 2000). Yet this seems to lead to a contradiction since

$$\langle v_z^p(t)\rangle/u_\eta = \langle u_z(\boldsymbol{x}^p(t), t)\rangle/u_\eta + Sv, \tag{2.3}$$

https://doi.org/10.1017/jfm.2019.337 Published online by Cambridge University Press

so that for $Sv = O(1)$, the particle settling becomes irrelevant to the mean motion of the particle in the limit $R_\lambda \to \infty$, yet the settling is supposed to be the very thing responsible for $\langle u_z(\boldsymbol{x}^p(t), t)\rangle \neq 0$. Clearly then new insight is needed to understand which scales of the turbulent flow influence $\langle u_z(\boldsymbol{x}^p(t), t)\rangle$, and we now develop a new theoretical framework to provide such insight.

2.2. *Theoretical framework for arbitrary St*

In this section we develop a theoretical framework for considering the behaviour of $\langle u_z(\boldsymbol{x}^p(t), t)\rangle$ for arbitrary St, and for revealing which scales of motion contribute to $\langle u_z(\boldsymbol{x}^p(t), t)\rangle \neq 0$.

In the analysis of Maxey (1987), attention was restricted to $St \ll 1$, for which it is possible to approximate $\boldsymbol{v}^p(t)$ as a field

$$\boldsymbol{v}^p(t) = (\boldsymbol{u}(\boldsymbol{x}, t) - St\tau_\eta[\boldsymbol{a}(\boldsymbol{x}, t) - \boldsymbol{g}])|_{x=\boldsymbol{x}^p(t)} + O(St^2), \tag{2.4}$$

where $\boldsymbol{x}$ is a fixed point in space (unlike $\boldsymbol{x}^p(t)$), and $\boldsymbol{a} \equiv \partial_t \boldsymbol{u} + (\boldsymbol{u} \cdot \nabla)\boldsymbol{u}$ is the fluid acceleration field. Using this field representation, Maxey was able to construct an expression for $\langle u_z(\boldsymbol{x}^p(t), t)\rangle$ using a continuity equation for the instantaneous particle number density. However, when $St \geqslant O(1)$, this field approximation for $\boldsymbol{v}^p(t)$ fundamentally breaks down due to the formation of caustics in the particle velocity distributions, wherein particle velocities at a given location become multivalued (Wilkinson & Mehlig 2005). Therefore, a quite different approach to that employed by Maxey (1987) must be sought in order to analyse $\langle u_z(\boldsymbol{x}^p(t), t)\rangle$ for arbitrary St.

We begin by noting that for homogeneous turbulence we may write

$$\langle u_z(\boldsymbol{x}^p(t), t)\rangle = \varrho^{-1}\langle u_z(\boldsymbol{x}, t)\delta(\boldsymbol{x}^p(t) - \boldsymbol{x})\rangle, \tag{2.5}$$

where $\delta(\cdot)$ is a Dirac distribution, and $\varrho \equiv \langle\delta(\boldsymbol{x}^p(t) - \boldsymbol{x})\rangle$ is the probability density function (PDF) of $\boldsymbol{x}^p(t)$. Here, $\langle\cdot\rangle$ is an ensemble average over all possible realizations of the system, and this includes not only an average over all realizations of $\boldsymbol{u}$, but also an average over all initial particle positions $\boldsymbol{x}^p(0) = \boldsymbol{x}_0$ and velocities $\boldsymbol{v}^p(0) = \boldsymbol{v}_0$. From (2.5) it follows that for a homogeneous turbulent flow, $\langle u_z(\boldsymbol{x}^p(t), t)\rangle = \langle u_z(\boldsymbol{x}, t)\rangle = 0$ if $\boldsymbol{x}^p(t)$ is uncorrelated with $u_z(\boldsymbol{x}, t)$. This occurs for $St \gg 1$ particles that move ballistically. It also occurs for fluid particles that are fully mixed at $t = 0$ (Bragg, Swailes & Skartlien 2012*b*), since their spatial distribution remains constant and uniform $\forall t$ due to incompressibility. In fact, $\langle u_z(\boldsymbol{x}^p(t), t)\rangle \neq 0$ can only occur if $\delta(\boldsymbol{x}^p(t) - \boldsymbol{x})$ both fluctuates in time and is also correlated with $u_z(\boldsymbol{x}, t)$.

To proceed with an analysis of $\langle u_z(\boldsymbol{x}^p(t), t)\rangle$ that applies for arbitrary St, we introduce the averaging decomposition $\langle\cdot\rangle = \langle\langle\cdot\rangle_{\boldsymbol{u}}^{\boldsymbol{x}_0,\boldsymbol{v}_0}\rangle^{\boldsymbol{u}}$ (Bragg, Swailes & Skartlien 2012*a*), where $\langle\cdot\rangle_{\boldsymbol{u}}^{\boldsymbol{x}_0,\boldsymbol{v}_0}$ denotes an average over all initial particle positions $\boldsymbol{x}^p(0) = \boldsymbol{x}_0$ and velocities $\boldsymbol{v}^p(0) = \boldsymbol{v}_0$ for a given realization of the fluid velocity field $\boldsymbol{u}$, and $\langle\cdot\rangle^{\boldsymbol{u}}$ denotes an average over all realizations of $\boldsymbol{u}$. Introducing this decomposition to (2.5) we have

$$\langle u_z(\boldsymbol{x}^p(t), t)\rangle = \varrho^{-1}\langle\langle u_z(\boldsymbol{x}, t)\delta(\boldsymbol{x}^p(t) - \boldsymbol{x})\rangle_{\boldsymbol{u}}^{\boldsymbol{x}_0,\boldsymbol{v}_0}\rangle^{\boldsymbol{u}} = \varrho^{-1}\langle u_z(\boldsymbol{x}, t)\varphi(\boldsymbol{x}, t)\rangle^{\boldsymbol{u}}, \tag{2.6}$$

where

$$\varphi(\boldsymbol{x}, t) \equiv \langle\delta(\boldsymbol{x}^p(t) - \boldsymbol{x})\rangle_{\boldsymbol{u}}^{\boldsymbol{x}_0,\boldsymbol{v}_0}, \tag{2.7}$$

and also $\varrho \equiv \langle\varphi(\boldsymbol{x}, t)\rangle^{\boldsymbol{u}}$. The reason for introducing this averaging decomposition is that it will allow us to introduce a particle velocity field that is valid for arbitrary St, unlike (2.4) that is only valid for $St \ll 1$.

https://doi.org/10.1017/jfm.2019.337 Published online by Cambridge University Press

The evolution equation for φ is given by

$$\partial_t \varphi + \nabla \cdot (\varphi \boldsymbol{\mathcal{V}}(\boldsymbol{x}, t)) = 0, \tag{2.8}$$

where

$$\boldsymbol{\mathcal{V}}(\boldsymbol{x}, t) \equiv \langle \boldsymbol{v}^p(t) \rangle_{\boldsymbol{x},\boldsymbol{u}}^{\boldsymbol{x}_0,\boldsymbol{v}_0}. \tag{2.9}$$

The particle velocity field $\boldsymbol{\mathcal{V}}(\boldsymbol{x}, t)$ differs fundamentally from the particle velocity field used in Maxey (1987), namely (2.4), since $\boldsymbol{\mathcal{V}}(\boldsymbol{x}, t)$ does not presume that $\boldsymbol{v}^p(t)$ is uniquely determined for $\boldsymbol{x}^p(t) = \boldsymbol{x}$ in a given realization of $\boldsymbol{u}$. Rather, $\boldsymbol{\mathcal{V}}(\boldsymbol{x}, t)$ is constructed as an average over different particle trajectories (each corresponding to different $\boldsymbol{x}_0, \boldsymbol{v}_0$) satisfying $\boldsymbol{x}^p(t) = \boldsymbol{x}$ in a given realization of $\boldsymbol{u}$. We also emphasize that both φ and $\boldsymbol{\mathcal{V}}$ are turbulent fields, in general, since they depend upon the evolution of the particular realization of $\boldsymbol{u}$ to which they correspond.

The solution to (2.8) may be written formally as

$$\varphi(\boldsymbol{x}, t) = \varphi(\boldsymbol{\mathcal{X}}(0|\boldsymbol{x}, t), 0) \exp\left(- \int_0^t \nabla \cdot \boldsymbol{\mathcal{V}}(\boldsymbol{\mathcal{X}}(s|\boldsymbol{x}, t), s)\, \mathrm{d}s \right), \tag{2.10}$$

where $\dot{\boldsymbol{\mathcal{X}}}(t) \equiv \boldsymbol{\mathcal{V}}(\boldsymbol{\mathcal{X}}(t), t)$, and the notation $s|\boldsymbol{x}, t$ denotes that the variable is measured at time s along a trajectory satisfying $\boldsymbol{\mathcal{X}}(t) = \boldsymbol{x}$. Note that $\nabla \cdot \boldsymbol{\mathcal{V}}(\boldsymbol{\mathcal{X}}(s|\boldsymbol{x}, t), s)$ is to be understood as

$$\nabla \cdot \boldsymbol{\mathcal{V}}(\boldsymbol{\mathcal{X}}(s|\boldsymbol{x}, t), s) \equiv \nabla \cdot \boldsymbol{\mathcal{V}}(\boldsymbol{y}, s)|_{\boldsymbol{y}=\boldsymbol{\mathcal{X}}(s|\boldsymbol{x},t)} \tag{2.11}$$

such that the operator $\nabla \cdot \{\}$ acts on the spatial coordinate of the field $\boldsymbol{\mathcal{V}}$ and not on the trajectory endpoint coordinate $\boldsymbol{x}$.

For simplicity, we will take $\varphi(\boldsymbol{\mathcal{X}}(0|\boldsymbol{x}, t), 0) = 1/\mathcal{D}$, corresponding to particles that are initially uniformly distributed throughout the volume $\mathcal{D}$ of the system (this was also assumed in Maxey (1987)). Further, we note that for a statistically stationary, homogeneous system, $\varrho\mathcal{D} = 1 \ \forall t$ when $\varphi(\boldsymbol{\mathcal{X}}(0|\boldsymbol{x}, t), 0) = 1/\mathcal{D}$. Using this initial condition for all realizations of $\boldsymbol{u}$, we may then insert (2.10) into (2.6) and obtain

$$\langle u_z(\boldsymbol{x}^p(t), t) \rangle = \left\langle u_z(\boldsymbol{x}, t) \exp\left(- \int_0^t \nabla \cdot \boldsymbol{\mathcal{V}}(\boldsymbol{\mathcal{X}}(s|\boldsymbol{x}, t), s)\, \mathrm{d}s \right) \right\rangle^{\boldsymbol{u}}. \tag{2.12}$$

Before proceeding, we note that in the regime $St \ll 1$ we may insert (2.4) into the definition of $\boldsymbol{\mathcal{V}}(\boldsymbol{x}, t)$ and obtain

$$\begin{aligned} \boldsymbol{\mathcal{V}}(\boldsymbol{x}, t) &= \langle \boldsymbol{u}(\boldsymbol{x}^p(t), t) - St\tau_\eta[\boldsymbol{a}(\boldsymbol{x}^p(t), t) - \boldsymbol{g}] \rangle_{\boldsymbol{x},\boldsymbol{u}}^{\boldsymbol{x}_0,\boldsymbol{v}_0} + O(St^2) \\ &= \boldsymbol{u}(\boldsymbol{x}, t) - St\tau_\eta[\boldsymbol{a}(\boldsymbol{x}, t) - \boldsymbol{g}] + O(St^2), \end{aligned} \tag{2.13}$$

and inserting this into (2.12) we obtain essentially the same result as Maxey (1987)

$$\langle u_z(\boldsymbol{x}^p(t), t) \rangle \approx \left\langle u_z(\boldsymbol{x}, t) \exp\left(St\tau_\eta \int_0^t (\mathcal{S}^2(\boldsymbol{x}^p(s|\boldsymbol{x}, t), s) - \mathcal{R}^2(\boldsymbol{x}^p(s|\boldsymbol{x}, t), s))\, \mathrm{d}s \right) \right\rangle^{\boldsymbol{u}}, \tag{2.14}$$

where $\mathcal{S}^2$ and $\mathcal{R}^2$ are the second invariants of the fluid strain-rate and rotation-rate tensors, respectively. The interpretation of (2.14) given by Maxey (1987) is that $\langle u_z(\boldsymbol{x}^p(t), t) \rangle > 0$ arises because settling inertial particles preferentially sweep around vortices where $\mathcal{S}^2 - \mathcal{R}^2 > 0$ due to the centrifuging effect, favouring the downward moving side of the vortices associated with $u_z > 0$.

https://doi.org/10.1017/jfm.2019.337 Published online by Cambridge University Press

Our result in (2.12), that is not restricted to $St \ll 1$, suggests more generally that $\langle u_z(\boldsymbol{x}^p(t), t)\rangle > 0$ can arise when $\boldsymbol{\mathcal{V}}(\boldsymbol{x}, t)$ is compressible, and also when there exists a correlation between regions where $\boldsymbol{\nabla}\cdot\boldsymbol{\mathcal{V}} < 0$ and $u_z > 0$. The argument given by Wang & Maxey (1993) for this correlation is essentially connected to the fact that settling particles typically approach the turbulent vortices from above as they fall through the flow, and they are swept around the vortices due to the centrifuge effect. A supplementary argument to theirs is that the settling particles tend to follow the 'path of least resistance'. In particular, downward moving particles prefer to move around the downward moving side of vortices in the flow since on this side they experience a weaker drag force ('less resistance') than they would if they were to fall around the upward moving side of the vortices.

Unlike the $St \ll 1$ regime, for $St \geqslant O(1)$, $\boldsymbol{\mathcal{V}}(\boldsymbol{x}, t)$ depends non-locally in time upon the fluid velocity field. Indeed, using the formal solution to (2.1) we may write (ignoring initial conditions)

$$\boldsymbol{\mathcal{V}}(\boldsymbol{x}, t) = St\tau_\eta \boldsymbol{g} + \frac{1}{St\tau_\eta}\int_0^t \mathrm{e}^{-(t-s)/St\tau_\eta}\langle \boldsymbol{u}(\boldsymbol{x}^p(s), s)\rangle_{\boldsymbol{x},\boldsymbol{u}}^{\boldsymbol{x}_0,\boldsymbol{v}_0}\,\mathrm{d}s, \tag{2.15}$$

so that $\boldsymbol{\mathcal{V}}(\boldsymbol{x}, t)$ depends on $\boldsymbol{u}$ at earlier times along the particle trajectory, and is in this sense temporally non-local. Due to this non-locality, there need not exist a correlation between $\boldsymbol{\nabla}\cdot\boldsymbol{\mathcal{V}}$ and the local properties of the flow. When $\boldsymbol{\nabla}\cdot\boldsymbol{\mathcal{V}}$ is uncorrelated with the fluid velocity field then from (2.12) we have

$$\begin{aligned}\langle u_z(\boldsymbol{x}^p(t), t)\rangle &= \left\langle u_z(\boldsymbol{x}, t)\exp\left(-\int_0^t \boldsymbol{\nabla}\cdot\boldsymbol{\mathcal{V}}(\boldsymbol{\mathcal{X}}(s|\boldsymbol{x}, t), s)\,\mathrm{d}s\right)\right\rangle^{\boldsymbol{u}} \\ &= \langle u_z(\boldsymbol{x}, t)\rangle^{\boldsymbol{u}}\left\langle\exp\left(-\int_0^t \boldsymbol{\nabla}\cdot\boldsymbol{\mathcal{V}}(\boldsymbol{\mathcal{X}}(s|\boldsymbol{x}, t), s)\,\mathrm{d}s\right)\right\rangle^{\boldsymbol{u}} \\ &= 0.\end{aligned} \tag{2.16}$$

Thus it is not merely clustering of the particles (related to $\boldsymbol{\nabla}\cdot\boldsymbol{\mathcal{V}} < 0$) that is required for $\langle u_z(\boldsymbol{x}^p(t), t)\rangle > 0$, but that the clustering be correlated in some way with the fluid velocity field. In view of this it is essential to make a distinction between two phenomena, namely particle clustering and preferential concentration. As emphasized in Bragg, Ireland & Collins (2015), these are distinct: clustering refers to non-uniformity of the particle spatial distribution, irrespective of any correlation the distribution may have with the fluid flow field. In contrast, preferential concentration describes the situation where the spatial distribution of the particles is not only non-uniform, but is also correlated to the local properties of the flow i.e. the particles cluster in specific regions of the flow, so that the particles preferentially sample the flow field. Recent results have shown that for settling particles this distinction is particularly important, since settling inertial particles can strongly cluster in the dissipation range of turbulence, despite the fact that their spatial distribution is entirely uncorrelated with the dissipation range properties of the turbulence (Ireland *et al.* 2016*b*). Indeed, while Ireland *et al.* (2016*b*) showed that the particle clustering (measured by the radial distribution function) becomes monotonically stronger at progressively smaller scales for all St, in § 4.4 we will show that the preferential sampling of the turbulent flow field is strongest at some intermediate flow scale that depends on St. This can occur because when $St \geqslant O(1)$, the mechanism that causes the particle clustering is not the centrifuge mechanism and the associated

https://doi.org/10.1017/jfm.2019.337 Published online by Cambridge University Press

preferential sampling of the flow field discussed in Maxey (1987), but rather a non-local mechanism that does not depend upon the particle interaction with the local fluid velocity field (Gustavsson & Mehlig 2011; Bragg & Collins 2014; Bragg *et al.* 2015; Bragg, Ireland & Collins 2015).

A subtle but important point that follows from this is that it is not in general appropriate to test the validity of the preferential sweeping mechanism by considering the particle settling velocities conditioned on the local particle concentration, as has often been done (Wang & Maxey 1993; Rosa & Pozorski 2017; Petersen *et al.* 2019). The reason is that, as pointed out above, it is preferential concentration, and not clustering (which is measured by local particle concentrations), that is connected with preferential sweeping and the enhanced particle settling speeds. The driver of the preferential sweeping mechanism is not the strength of the clustering (quantified by the local concentration), but the degree to which the particle locations are correlated with the local flow, i.e. preferential concentration. However, as discussed above, when $St \geqslant O(1)$, the clustering of settling particles may not be correlated with the local flow, and therefore analysing the particle settling velocities conditioned on the local particle concentration no longer provides a meaningful test of the validity of the preferential sweeping mechanism. It is interesting to note that Rosa & Pozorski (2017) observed that particle settling velocities increase with increasing local particle concentration for low inertia particles, but an opposite and weaker trend was observed for high inertia particles. This reversal in trend was attributed to the loitering effect and the ineffectiveness of the preferential sweeping mechanism for higher inertia particles. While this interpretation in terms of loitering may be valid, the differing behaviour observed for low and high St may be simply a reflection of the fact that while the settling velocity conditioned on concentration is an appropriate measure of settling velocity enhancement for $St \ll 1$, it is not for $St \geqslant O(1)$, as explained before.

2.3. *Multiscale insight*

Having constructed an expression for $\langle u_z(\boldsymbol{x}^p(t), t)\rangle$ in (2.12) that is valid for arbitrary St, we now develop the result further in order to gain insight into the multiscale nature of the problem. To do this, we introduce the coarse-graining decompositions $u_z(\boldsymbol{x}, t) = \widetilde{u}_z(\boldsymbol{x}, t) + u_z'(\boldsymbol{x}, t)$ and $\boldsymbol{\mathcal{V}} = \widetilde{\boldsymbol{\mathcal{V}}} + \boldsymbol{\mathcal{V}}'$, where $\widetilde{u}_z$ and $\widetilde{\boldsymbol{\mathcal{V}}}$ denote the fields u_z and $\boldsymbol{\mathcal{V}}$ coarse grained on the length scale $\ell_c(St)$, while $u_z'(\boldsymbol{x}, t) \equiv u_z(\boldsymbol{x}, t) - \widetilde{u}_z(\boldsymbol{x}, t)$ and $\boldsymbol{\mathcal{V}}' \equiv \boldsymbol{\mathcal{V}} - \widetilde{\boldsymbol{\mathcal{V}}}$ are the 'subgrid' fields. Inserting these decompositions into (2.12) we obtain

$$\begin{aligned}\langle u_z(\boldsymbol{x}^p(t), t)\rangle &= \left\langle \widetilde{u}_z(\boldsymbol{x}, t) \exp\left(-\int_0^t (\boldsymbol{\nabla}\cdot\widetilde{\boldsymbol{\mathcal{V}}}(\boldsymbol{\mathcal{X}}(s|\boldsymbol{x}, t), s) + \boldsymbol{\nabla}\cdot\boldsymbol{\mathcal{V}}'(\boldsymbol{\mathcal{X}}(s|\boldsymbol{x}, t), s))\,\mathrm{d}s\right)\right\rangle^{\boldsymbol{u}} \\ &\quad + \left\langle u_z'(\boldsymbol{x}, t) \exp\left(-\int_0^t (\boldsymbol{\nabla}\cdot\widetilde{\boldsymbol{\mathcal{V}}}(\boldsymbol{\mathcal{X}}(s|\boldsymbol{x}, t), s) + \boldsymbol{\nabla}\cdot\boldsymbol{\mathcal{V}}'(\boldsymbol{\mathcal{X}}(s|\boldsymbol{x}, t), s))\,\mathrm{d}s\right)\right\rangle^{\boldsymbol{u}}. \end{aligned} \tag{2.17}$$

We now consider the Taylor Reynolds number $R_\lambda \to \infty$, and choose the coarse-graining length scale $\ell_c(St)$ to be a function of St, i.e. $\ell_c(St)$. To do this, we define the scale-dependent Stokes number $St_\ell \equiv \tau_p/\tau_\ell$, where τ_ℓ is the eddy turnover time scale at scale ℓ. We then define $\ell_c(St)$ through $St_{\ell_c} = \gamma$, where γ is a constant such that $\gamma \lll 1$. With this definition, $\ell \geqslant \ell_c(St)$ corresponds to flow scales at which the effects of the particle inertia are negligibly small, and the effects of particle

https://doi.org/10.1017/jfm.2019.337 Published online by Cambridge University Press

inertia are only felt at scales $\ell < \ell_c(St)$. Since τ_ℓ is a non-decreasing function of ℓ in homogeneous turbulence, it follows that $\ell_c(St)$ is a non-decreasing function of St. In order to illustrate more clearly the connection between ℓ_c and St, we may use Kolmogorov's 1941 theory, K41 Pope (2000) to derive their relationship for the case where ℓ_c lies in the inertial range. From K41 we have that for ℓ in the inertial range $\tau_\ell \sim \langle\epsilon\rangle^{-1/3}\ell^{2/3}$, and then using the definition of $\ell_c(St)$ we obtain $\ell_c(St) \sim \eta(St/\gamma)^{3/2}$. This then shows how as St is increased, $\ell_c(St)$ also increases.

According to the definition of $\ell_c(St)$, the particle clustering at scales $\ell \geqslant \ell_c(St)$ is negligible and therefore

$$\exp\left(-\int_0^t \boldsymbol{\nabla}\cdot\widetilde{\boldsymbol{\mathcal{V}}}(\boldsymbol{\mathcal{X}}(s|\boldsymbol{x},t),s)\,\mathrm{d}s\right)\approx 1, \tag{2.18}$$

such that the contribution in (2.17) associated with fluctuations of the particle concentration field $\varphi(\boldsymbol{x},t)$ arises only from the subgrid contribution $\exp(-\int_0^t \boldsymbol{\nabla}\cdot\boldsymbol{\mathcal{V}}'(\boldsymbol{\mathcal{X}}(s|\boldsymbol{x},t),s)\,\mathrm{d}s)$. Further, since $\gamma \lll 1$, significant deviations of $\boldsymbol{\nabla}\cdot\boldsymbol{\mathcal{V}}'$ from zero will only occur at scales $\ell \ll \ell_c(St)$, and therefore $\boldsymbol{\nabla}\cdot\boldsymbol{\mathcal{V}}'$ should be uncorrelated with $\widetilde{u}_z(\boldsymbol{x},t)$, under the standard assumption that widely separated flow scales in turbulence are uncorrelated. This assumption, together with (2.18), reduces (2.17) to the result

$$\langle u_z(\boldsymbol{x}^p(t),t)\rangle \approx \left\langle u_z'(\boldsymbol{x},t)\exp\left(-\int_0^t \boldsymbol{\nabla}\cdot\boldsymbol{\mathcal{V}}'(\boldsymbol{\mathcal{X}}(s|\boldsymbol{x},t),s)\,\mathrm{d}s\right)\right\rangle^{\boldsymbol{u}}. \tag{2.19}$$

Since the right-hand side of this result only contains the subgrid fields, it shows that the particle settling speeds are not affected by every scale of the turbulent flow. Instead, only scales of size $\ell < \ell_c(St)$ contribute to the enhanced settling due to turbulence. The physical mechanism embedded in (2.19) is a multiscale version of the original preferential sweeping mechanism described by Maxey (1987) and Wang & Maxey (1993). In particular, according to (2.19), $\langle u_z(\boldsymbol{x}^p(t),t)\rangle > 0$ occurs because the inertial particles are preferentially swept by eddies of size $\ell < \ell_c(St)$.

2.4. *Implications of result*

A number of interesting and important implications and predictions follow from (2.19), which we now discuss.

2.4.1. *The scales of motion that influence the particle settling speed*

The result in (2.19) shows that the turbulent flow scales that contribute to the enhanced particle settling speeds are those with size less than $\ell_c(St)$, while scales of size greater than or equal to $\ell_c(St)$ make a negligible contribution. Since $\ell_c(St)$ is a non-decreasing function of St then it follows that increasingly larger scales contribute to the enhanced settling speeds as St is increased.

One important implication of this is that there cannot, on theoretical grounds, be any single flow scale that determines $\langle u_z(\boldsymbol{x}^p(t),t)\rangle$. This is in contrast to previous work (e.g. Wang & Maxey 1993; Yang & Lei 1998; Good *et al.* 2014; Nemes *et al.* 2017) where it has been argued that the relevant velocity scale determining $\langle u_z(\boldsymbol{x}^p(t),t)\rangle$ is u', which is associated with the large scales of the flow. We would argue that the results in those previous studies were strongly affected by the fact that the R_λ values they considered were such that u'/u_η was not very large.

According to (2.19), the flow scales that determine $\langle u_z(\boldsymbol{x}^p(t),t)\rangle$ depend essentially upon St, and when $St \ll 1$, we expect $\ell_c(St) = O(\eta)$ so that $\langle u_z(\boldsymbol{x}^p(t),t)\rangle$ depends on

https://doi.org/10.1017/jfm.2019.337 Published online by Cambridge University Press

u_η, not u'. On the other hand, when $1 \ll St \ll \tau_L/\tau_\eta$ (where τ_L is the integral time scale of the flow), the velocity scale dominating $\langle u_z(\boldsymbol{x}^p(t), t)\rangle$ will correspond to those of inertial range eddies that have velocities much greater than u_η, but much less than u' (when $R_\lambda \to \infty$).

2.4.2. *Influence of R_λ on the particle settling speed*

Another implication of (2.19) concerns the influence of R_λ on $\langle u_z(\boldsymbol{x}^p(t),\ t)\rangle$. According to K41 (Pope 2000), the velocity scale associated with an eddy of size ℓ, i.e. $\mathcal{U}(\ell)$, grows as $\mathcal{U}(\ell) \propto \ell$ in the dissipation range, $\mathcal{U}(\ell) \propto \ell^{1/3}$ in the inertial range, and for $\ell > L$ we have $\mathcal{U}(\ell) = u'$, where L is the integral length scale of the flow. Further, using K41 we also have $\mathcal{U}(\ell \geqslant L)/u_\eta \propto R_\lambda^{1/2}$. In figure 1, we plot $\mathcal{U}(\ell)/u_\eta$ for four different values of R_λ (these curves are plotted using the curve fit for $\mathcal{U}(\ell)$ in Zaichik & Alipchenkov (2009)), and we denote the integral length scales for these flows as L_1, L_2, L_3, L_4, where $L_1 < L_2 < L_3 < L_4$ (we assume η is the same for each flow for simplicity of the discussion). Also indicated using dashed lines are two values of $\ell_c(St)$ corresponding to Stokes numbers St_1 and St_2 where $St_1 < St_2$ so that $\ell_c(St_1) < \ell_c(St_2)$. An important point is that when normalized by the Kolmogorov scales, $\mathcal{U}(\ell)$ is independent of R_λ when $\ell < L_1$. Indeed a consequence of K41 is that when considering any two turbulent flows, $\mathcal{U}(\ell)/u_\eta$ will be independent of R_λ up to scales where ℓ is of the order of the integral length scale of the flow that has the smallest R_λ.

Now, let us consider how $\langle u_z(\boldsymbol{x}^p(t), t)\rangle/u_\eta$ would vary across these four R_λ values for St_1 and St_2. For St_1, since $\ell_c(St_1) < L_1$ then $\langle u_z(\boldsymbol{x}^p(t), t)\rangle/u_\eta$ should be independent of R_λ since $\mathcal{U}(\ell)/u_\eta$ is the same for each of the flows until $\ell \geqslant L_1$. On the other hand, for St_2, $\langle u_z(\boldsymbol{x}^p(t), t)\rangle/u_\eta$ will differ for the smallest two values of R_λ since $\ell_c(St_2) > L_2$. However, for the largest two values of R_λ, $\langle u_z(\boldsymbol{x}^p(t), t)\rangle/u_\eta$ should be the same since $\ell_c(St_2) < L_3$. In other words, the R_λ dependence of $\langle u_z(\boldsymbol{x}^p(t), t)\rangle/u_\eta$ for St_2 will saturate once the integral length scale of the flow, $L(R_\lambda)$, exceeds $\ell_c(St_2)$.

More generally, $\langle u_z(\boldsymbol{x}^p(t), t)\rangle/u_\eta$ will only depend on R_λ while $\ell_c(St) > L(R_\lambda)$. For finite St, $\ell_c(St)$ is always finite, and therefore for $R_\lambda \to \infty$, the R_λ dependence of $\langle u_z(\boldsymbol{x}^p(t), t)\rangle/u_\eta$ will always saturate for all finite St.

2.4.3. *Influence of Froude number on the scales governing particle settling speeds*

Usually, preferential concentration at scale ℓ is said to be strongest when $St_\ell = O(1)$. However, in the presence of gravity, this needs to be nuanced. In particular, we should instead say that preferential concentration at scale ℓ is strongest when $St\tau_\eta = O(T_\ell)$, where T_ℓ is the eddy turnover time scale seen by the particle, which depends upon St and Fr, and, like τ_ℓ, is a non-decreasing function of ℓ. For a given St and ℓ, T_ℓ decreases with decreasing Fr, reflecting the fact that the faster a particle falls through the flow, the faster the fluid velocity along its trajectory will decorrelate. This then means that for a given St, as Fr is decreased, one has to go to larger flow scales in order to observe $St\tau_\eta = O(T_\ell)$. Now suppose we redefine $\ell_c(St)$ using T_ℓ instead of τ_ℓ, by defining $\ell_c(St)$ through $St\tau_\eta/T_{\ell_c} = \gamma$, and again take $\gamma \lll 1$. With this definition we observe that for fixed St, $\ell_c(St)$ increases with decreasing Fr, i.e. as Fr is decreased, one has to go to larger values of ℓ in order to satisfy $St\tau_\eta/T_\ell = \gamma$. Through (2.19), this then means that as Fr is decreased, the scales contributing to the particle settling enhancement increase.

3. Testing the arguments using DNS data

We will test the theoretical arguments presented in the previous section using DNS data spanning a range of R_λ, St and Fr.

https://doi.org/10.1017/jfm.2019.337 Published online by Cambridge University Press

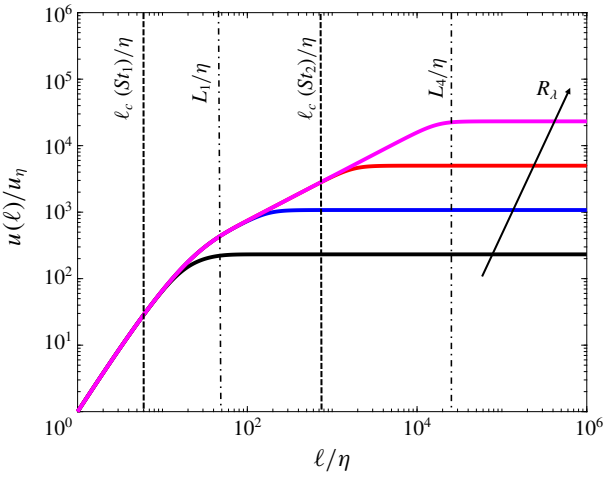


FIGURE 1. (Colour online) Plot to illustrate how $\ell_c(St)$ determines the R_λ dependence of $\langle u_z(\boldsymbol{x}^p(t), t)\rangle$. The values of R_λ shown correspond to $R_\lambda = [29, 133, 615, 2854]$.

3.1. *DNS details*

Our DNS dataset is identical to that in Ireland, Bragg & Collins (2016*a*), Ireland *et al.* (2016*b*), and we therefore refer the reader to that paper for the details of the DNS. Here we just give a brief summary. We perform a pseudo-spectral DNS of isotropic turbulence on a three-dimensional triperiodic cube of length $\mathcal{L}$ with N^3 grid points. The Navier–Stokes equation for an incompressible fluid was solved, with the pressure term eliminated using the divergence-free condition for the velocity field.

$$\boldsymbol{\nabla}\cdot\boldsymbol{u} = 0, \tag{3.1}$$

$$\frac{\partial \boldsymbol{u}}{\partial t} + \boldsymbol{\omega}\times\boldsymbol{u} + \boldsymbol{\nabla}\left(\frac{P}{\rho_f} + \frac{u^2}{2}\right) = \nu\nabla^2\boldsymbol{u} + \boldsymbol{f}, \tag{3.2}$$

where $\boldsymbol{u}$ is the fluid velocity, $\boldsymbol{\omega}$ is the vorticity, P is the pressure, ρ_f is the fluid density, ν is the kinematic viscosity and $\boldsymbol{f}$ is a large scale forcing term that is added to make the flow field statistically stationary. Deterministic forcing was applied to wavenumbers with magnitude $k = \sqrt{2}$. A detailed description of the numerical methods used can be found in Ireland *et al.* (2013). The gravity term in the Navier–Stokes equation is precisely cancelled by the mean pressure gradient and so it has no dynamical consequence on the turbulent flow field. When using periodic boundary conditions, particles can artificially re-encounter the same large eddy as they are periodically looped through the domain, if the time it takes the settling particles to traverse the distance $\mathcal{L}$ is smaller than the large-eddy turnover time, i.e. if $\mathcal{L}/St\tau_\eta g < O(\tau_L)$. In all of our simulations, the domain lengths $\mathcal{L}$ are chosen to satisfy $\mathcal{L}/St\tau_\eta g > \tau_L$, thereby suppressing the artificial periodicity effects for settling particles (a systematic study of this was presented in Ireland *et al.* (2016*b*)).

In order to analyse the same dynamical system we considered in the theory, we track inertial particles governed by (2.1), where particles are acted upon by both gravity and linear drag force. We assume that the particle loading is dilute and hence interparticle interactions and two-way coupling can be neglected (Elghobashi & Truesdell 1993; Sundaram & Collins 1997). An eight-point B-spline interpolation

https://doi.org/10.1017/jfm.2019.337 Published online by Cambridge University Press

Simulation	I	II	III	IV	V	VI
R_λ	90	224	230	237	398	398
Fr	0.052	∞	0.052	0.3	∞	0.052
$\mathcal{L}$	16π	2π	4π	2π	2π	2π
N	1024	512	1024	512	1024	1024
ν	0.005	0.0008289	0.0008289	0.0008289	0.0003	0.0003
$\langle\epsilon\rangle$	0.257	0.253	0.239	0.2842	0.223	0.223
L	1.47	1.40	1.49	1.43	1.45	1.45
L/η	55.6	204	213	214	436	436
u'	0.912	0.915	0.914	0.966	0.915	0.915
u'/u_η	4.82	7.60	7.70	7.82	10.1	10.1
τ_L	1.61	1.53	1.63	1.48	1.58	1.58
τ_L/τ_η	11.52	26.8	27.66	27.36	43.0	43.0
$k_{max}\eta$	1.61	1.66	1.68	1.62	1.60	1.60
N_p	16 777 216	2 097 152	16 777 216	2 097 152	2 097 152	2 097 152

TABLE 1. Flow parameters in DNS of isotropic turbulence where all dimensional parameters are in arbitrary units and all statistics are averaged over the duration of the run (T).$R_\lambda \equiv u'\lambda/\nu \equiv 2k/\sqrt{5/3\nu\langle\epsilon\rangle}$ is the Taylor microscale Reynolds number, Fr is the Froude number, λ is the Taylor microscale, $\mathcal{L}$ is the domain size, N is the number of grid points in each direction, ν is the fluid kinematic viscosity, $\langle\epsilon\rangle \equiv 2\nu\int_0^{\kappa_{max}}\kappa^2 E(\kappa)\,\mathrm{d}\kappa$ is the mean turbulent kinetic energy dissipation rate, κ is the wavenumber in Fourier space, E is the energy spectrum, $L \equiv (3\pi/2k)(\int_0^{\kappa_{max}}(E(\kappa)/\kappa)\,\mathrm{d}\kappa)$ is the integral length scale, $\eta \equiv (\nu^3/\langle\epsilon\rangle)^{1/4}$ is the Kolmogorov length scale, $u' \equiv \sqrt{2k/3}$ is the r.m.s. of fluctuating fluid velocity, k is the turbulent kinetic energy, $u_\eta \equiv (\langle\epsilon\rangle\nu)^{3/4}$ is the Kolmogorov velocity scale, $\tau_L \equiv L/u'$ is the large-eddy turnover time, $\tau_\eta \equiv \sqrt{\nu/\langle\epsilon\rangle}$ is the Kolmogorov time scale, $k_{max} = \sqrt{2}N/3$ is the maximum resolved wavenumber and N_p is the number of particles per Stokes number used in the simulation. The grid spacing is kept constant as the domain size is increased, and so the small scale resolution, $k_{max}\eta$, is approximately constant between the different domain sizes. The viscosity and forcing parameters were kept the same when increasing domain size, and thus both small scale and large scale flow parameters are held approximately constant.

scheme (with C^6 continuity) based on the algorithm in van Hinsberg *et al.* (2012) was used to compute the fluid velocity at the particle position, $u(\boldsymbol{x}^p(t), t)$. We consider $R_\lambda = 90$, 230 and 398 (note that we refer to the simulations with $R_\lambda = 224$, 230, 237 nominally as having $R_\lambda \approx 230$ since they differ only due to statistical fluctuations, but correspond to the same ν) and two Fr that are representative of the conditions in clouds, $Fr = 0.052$ for a cumulus clouds and $Fr = 0.3$ for a strongly turbulent cumulonimbus cloud (see Ireland *et al.* 2016*b*). Fourteen different particle classes are simulated with $St \in [0, 2]$. Details of the simulations are given in table 1. Note that the data for $R_\lambda = 237$ and $Fr = 0.3$ are from Momenifar, Dhariwal & Bragg (2018), while the rest are from Ireland *et al.* (2016*a*,*b*).

3.2. *Testing methodology*

It would be very difficult to directly test (2.19) owing to the practical difficulty in constructing the field $\boldsymbol{\mathcal{V}}'(\boldsymbol{x}, t)$ (and a simple evolution equation for $\boldsymbol{\mathcal{V}}'(\boldsymbol{x}, t)$ is not available). However, the insights and predictions from the theoretical analysis can be tested by computing $\langle u_z'(\boldsymbol{x}^p(t), t)\rangle$ for various coarse-graining length scales, and

https://doi.org/10.1017/jfm.2019.337 Published online by Cambridge University Press

analysing how the coarse graining affects the results for varying St, R_λ and Fr. Strictly speaking, $\langle u_z'(\boldsymbol{x}^p(t), t)\rangle$ does not actually correspond to (2.19), but rather corresponds to (2.19) with $\boldsymbol{\nabla}\cdot\boldsymbol{\mathcal{V}}'$ replaced by $\boldsymbol{\nabla}\cdot\boldsymbol{\mathcal{V}}$. However, according to the arguments and definitions leading to (2.19), these two quantities are asymptotically equivalent since the coarse-graining length scale ℓ_c is defined in such a way that $\boldsymbol{\nabla}\cdot\boldsymbol{\mathcal{V}}'\approx\boldsymbol{\nabla}\cdot\boldsymbol{\mathcal{V}}$ since $|\boldsymbol{\nabla}\cdot\widetilde{\boldsymbol{\mathcal{V}}}|\lll|\boldsymbol{\nabla}\cdot\boldsymbol{\mathcal{V}}'|$. Therefore, comparing $\langle u_z'(\boldsymbol{x}^p(t), t)\rangle$ with the implications and predictions following from (2.19) is appropriate.

To take full advantage of our existing large database on inertial particle motion in isotropic turbulence (see Ireland *et al.* 2016*a*,*b*), we compute $\langle u_z'(\boldsymbol{x}^p(t), t)\rangle$ from our existing DNS data via postprocessing. To do this we take our DNS data for $u_z(\boldsymbol{x}, t)$ and the particle positions $\boldsymbol{x}^p(t)$ at a number of different times, for multiple St, R_λ and Fr. We then apply a sharp spectral cutoff at wavenumber k_F to $u_z(\boldsymbol{x}, t)$, and from this obtain the subgrid field through

$$u_z'(\boldsymbol{x}, t)\equiv u_z(\boldsymbol{x}, t)-\widetilde{u}_z(\boldsymbol{x}, t)=\sum_{\|\boldsymbol{k}\|>k_F}\hat{u}_z(\boldsymbol{k}, t)\mathrm{e}^{\mathrm{i}\boldsymbol{k}\cdot\boldsymbol{x}}, \tag{3.3}$$

where here and throughout, $\widetilde{(\cdot)}$ denotes the coarse-grained field, while $(\cdot)'$ denotes the subgrid field. We then interpolate $u_z'(\boldsymbol{x}, t)$ to the positions of inertial particles $\boldsymbol{x}^p(t)$ using an eighth-order B-spline interpolation scheme to obtain $u_z'(\boldsymbol{x}^p(t), t)$. The values of $u_z'(\boldsymbol{x}^p(t), t)$ are then averaged over all the particles (with a given St) and over multiple times to obtain $\langle u_z'(\boldsymbol{x}^p(t), t)\rangle$. This process is then repeated for multiple k_c in order to examine the effect of the coarse graining and how its effect depends on St, R_λ and Fr. In order to relate the spectral cutoff wavenumber k_F to a physical space filtering scale we define $\ell_F\equiv 2\pi/k_F$ (Eyink & Aluie 2009).

By considering the results of $\langle u_z'(\boldsymbol{x}^p(t), t)\rangle$ for various St, ℓ_F, Fr and R_λ and comparing them with those for $\langle u_z(\boldsymbol{x}^p(t), t)\rangle$, we can test the predictions of the theory regarding which flow scales contribute to $\langle u_z(\boldsymbol{x}^p(t), t)\rangle$.

4. Results and discussion

4.1. *The scales of motion that influence the particle settling speed*

The theoretical analysis predicts that the range of scales that contribute to $\langle u_z(\boldsymbol{x}^p(t), t)\rangle$ should monotonically increase as St increases. To test this prediction, in figure 2, we plot the ratio $\langle u_z'(\boldsymbol{x}^p(t), t)\rangle/\langle u_z(\boldsymbol{x}^p(t), t)\rangle$ for various filtering length scales ℓ_F, and various R_λ. For $St\lll 1$ we would have $\ell_c(St)=O(\eta)$, and so filtering out scales $\ell_F>O(\eta)$ would have little effect, since the particle settling speed is only affected by the scales less than $\ell_c(St)$. Hence, for $St\lll 1$, we expect $\langle u_z'(\boldsymbol{x}^p(t), t)\rangle/\langle u_z(\boldsymbol{x}^p(t), t)\rangle\approx 1$. On the other hand, for $St=O(1)$ we would have $\ell_c(St)>O(\eta)$, and so filtering out scales $\ell_F>O(\eta)$ would have a strong effect, since these scales make a strong contribution to the particle settling speed. Hence, for $St=O(1)$, we expect $\langle u_z'(\boldsymbol{x}^p(t), t)\rangle/\langle u_z(\boldsymbol{x}^p(t), t)\rangle\ll 1$. More generally, the prediction is that for a given ℓ_F, $\langle u_z'(\boldsymbol{x}^p(t), t)\rangle/\langle u_z(\boldsymbol{x}^p(t), t)\rangle$ should decrease with increasing St, reflecting the fact that $\langle u_z(\boldsymbol{x}^p(t), t)\rangle$ is affected by increasingly larger scales as St is increased. The results in figure 2 confirm this prediction. They also reveal how sensitive $\langle u_z(\boldsymbol{x}^p(t), t)\rangle$ is to scales $\ell\gg\eta$, even when $St=O(0.1)$, which is quite surprising.

To further illustrate this behaviour, in figure 3, we plot $\langle u_z'(\boldsymbol{x}^p(t), t)\rangle/\langle u_z(\boldsymbol{x}^p(t), t)\rangle$ as a function of ℓ_F/η for various St. For $St\lesssim 0.2$ we clearly see that as ℓ_F is increased, $\langle u_z'(\boldsymbol{x}^p(t), t)\rangle$ approaches a constant value, implying that there do indeed exist scales beyond a certain size that have a negligible effect on the particle settling velocity, as

https://doi.org/10.1017/jfm.2019.337 Published online by Cambridge University Press

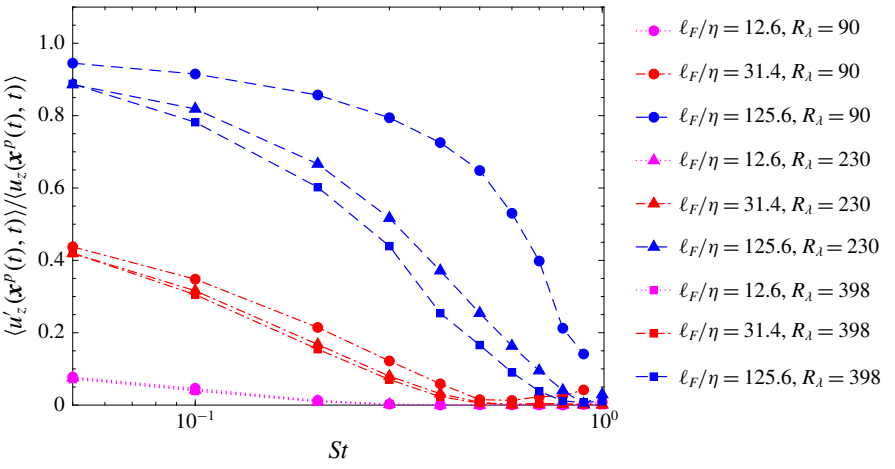


FIGURE 2. (Colour online) DNS results for $\langle u_z'(\boldsymbol{x}^p(t),t)\rangle/\langle u_z(\boldsymbol{x}^p(t),t)\rangle$ as a function of St, for $Fr = 0.052$, and for various filtering lengths ℓ_F/η. The circles correspond to $R_\lambda = 90$, the triangles to $R_\lambda \approx 230$ and the squares to $R_\lambda = 398$. The dashed lines correspond to $\ell_F/\eta = 125.6$, the dash-dot lines to $\ell_F/\eta = 31.4$, and the dotted lines to $\ell_F/\eta = 12.6$.

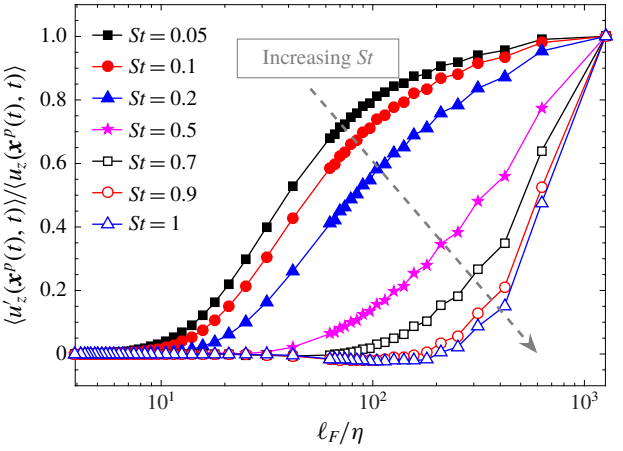


FIGURE 3. (Colour online) DNS data for $\langle u_z'(\boldsymbol{x}^p(t),t)\rangle/\langle u_z(\boldsymbol{x}^p(t),t)\rangle$ as a function of ℓ_F/η for different St, and $Fr = 0.052$, $R_\lambda = 398$.

predicted by the theory. However, for $St = O(1)$, we do not see such an asymptote, and their settling velocity is significantly affected by the largest scales in the flow. In order to understand why this is the case, we will now estimate $\ell_c(St)$.

Recall that in the derivation of our theoretical result we prescribed the parameter γ to have the asymptotic value $\gamma \lll 1$. However, we may estimate a value for γ from our DNS. To do this, we note that for $St = 0.05$, $\langle u_z'(\boldsymbol{x}^p(t),t)\rangle/\langle u_z(\boldsymbol{x}^p(t),t)\rangle \approx 1$ for $\ell_F/\eta \gtrsim 600$ and hence $\ell_c(St = 0.05) \approx 600\eta$. Then using the K41 result discussed earlier, $\ell_c(St) \sim \eta(St/\gamma)^{3/2}$ and using $\ell_c(St = 0.05) \approx 600\eta$, we obtain the estimate $\gamma \approx 7 \times 10^{-4}$. Using this value, in figure 4 we plot $\ell_c(St) \sim \eta(St/\gamma)^{3/2}$, where we have taken $R_\lambda \to \infty$ so that the inertial range scaling $\ell_c(St) \sim \eta(St/\gamma)^{3/2}$ applies for all $St \geqslant 0.05$. Using this estimated behaviour we find that for $St = 1$, $\ell_c(St)/\eta \approx 5.4 \times 10^4$.

https://doi.org/10.1017/jfm.2019.337 Published online by Cambridge University Press

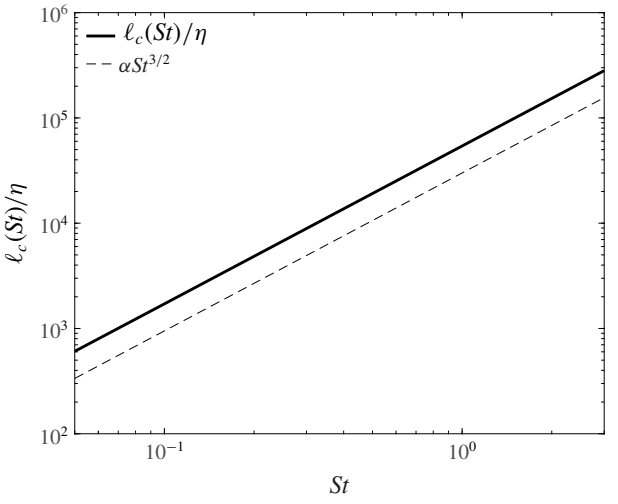


FIGURE 4. Plot illustrating how $\ell_c(St)/\eta$ grows with St.

In our DNS at $R_\lambda = 398$, the ratio of the integral length scale L to η is $L/\eta = 4.3 \times 10^2$ which is two orders of magnitude smaller than $\ell_c(St)/\eta$ for $St = 1$. This then explains why in our DNS we do not observe a saturation of $\langle u_z'(\boldsymbol{x}^p(t), t)\rangle / \langle u_z(\boldsymbol{x}^p(t), t)\rangle$ for $St = O(1)$ as ℓ_F is increased. An important conclusion that follows from this is that while the settling speed of particles is dominated by a restricted range of scales, namely scales of size less than $\ell_c(St)$, this range can actually be quite large. Indeed, figure 4, and the results in figure 3 indicate that even for $St = 0.1$, $\ell_c(St)/\eta \approx 1.7 \times 10^3$ such that their settling speeds are affected by scales much larger than those in the dissipation range.

These findings also explain why in many previous numerical and experimental studies, it was found that $\langle u_z(\boldsymbol{x}^p(t), t)\rangle$ had a strong dependence on u', the large scale fluid velocity scale. We have argued that on theoretical grounds, $\langle u_z(\boldsymbol{x}^p(t), t)\rangle$ cannot be characterized by a single flow scale since the range of scales contributing to $\langle u_z(\boldsymbol{x}^p(t), t)\rangle$ depends on St. However, in these previous works R_λ was sufficiently small so that the particle settling speeds were significantly affected by all scales, and as a result $\langle u_z(\boldsymbol{x}^p(t), t)\rangle$ was found to have a strong dependence on u'. In contrast, in natural flows where R_λ is much larger, this would not be the case. In the atmosphere, typical values are $\eta = O(mm)$ and $L = O(100\ \text{m})$ (Shaw 2003; Grabowski & Wang 2013), and together with the results in figure 4 this implies we would have, for example, $\ell_c(St = 0.1) \approx 1.7$ m and $\ell_c(St = 1) \approx 54$ m. Consequently, for $St \leqslant 1$, the large scale fluid velocities in the atmosphere, characterized by u', would play no role in the particle settling. Nevertheless, the estimate $\ell_c(St = 1) \approx 54$ m shows that the range of atmospheric flow scales that may contribute to the enhanced settling speeds due to turbulence is quite large. This means that for $St = O(1)$, particle settling in the atmosphere may be strongly influenced by non-ideal effects such as flow inhomogeneity, anisotropy and stratification (noting that the Ozmidov scale is greater than or equal to $O(m)$ in the atmosphere (Riley & Lindborg 2012)).

So far we have emphasized that as St is increased, larger scales contribute to the particle settling since $\ell_c(St)$ is a non-decreasing function of St. However, in reality, as St is increased, not only do larger scales contribute to the particle settling, but

https://doi.org/10.1017/jfm.2019.337 Published online by Cambridge University Press

smaller scales begin to contribute less. This is because the preferential sweeping effect at any scale is only effective when $St_\ell \lll 1$ and $St_\ell \ggg 1$. Let us define $\widehat{\ell}_c(St)$ as the scale below which the preferential sweeping mechanism is not effective, so that scales $\ell < \widehat{\ell}_c(St)$ correspond to scales at which $St_\ell \ggg 1$. Then, the scales at which the preferential sweeping mechanism would operate are $\widehat{\ell}_c(St) \leqslant \ell < \ell_c(St)$, and both $\widehat{\ell}_c(St)$ and $\ell_c(St)$ are non-decreasing functions of St. While our theoretical analysis could be extended to also include the lower limit scale $\widehat{\ell}_c(St)$, we have chosen not to do so since it would render the theoretical result much more complicated. Furthermore, our principle concern in this paper is to understand the upper limit of the turbulent flow scales that contribute to the particle settling velocity in a turbulent flow, and this is given by $\ell_c(St)$. Nevertheless, understanding the minimum flow scales affecting the settling process is key to the development of particle subgrid scale (SGS) models for LES of particles settling in turbulent flows. The effect of the smallest scales of the turbulence on particle settling speeds was investigated by Rosa & Pozorski (2017) using DNS and their results showed that scales smaller than a certain size did not affect the particle settling speeds. Although their data do not provide enough information to determine exactly how this 'cutoff scale' depends on St, their data are consistent with our theoretical prediction that $\widehat{\ell}_c(St)$ is a non-decreasing function of St.

4.2. *Influence of R_λ on the particle settling speed*

As discussed in § 2.4.2, as R_λ is increased, the range of scales in the turbulent flow increases. According to our theoretical analysis, when $St \lll 1$, $\ell_c(St)$ is small enough so that the particles are not influenced by the additional scales introduced by increasing R_λ. Consequently, $\langle u_z(\boldsymbol{x}^p(t), t)\rangle$ should not vary with R_λ for $St \lll 1$. However, as St is increased, so also does $\ell_c(St)$, and for sufficiently large St, this allows the particles to feel the effects of the additional flow scales introduced by increasing R_λ. As a result, $\langle u_z'(\boldsymbol{x}^p(t), t)\rangle$ can depend on R_λ as St is increased. The results in figure 5 confirm this picture and show that without filtering (i.e. $\ell_F/\eta = \infty$), $\langle u_z'(\boldsymbol{x}^p(t), t)\rangle = \langle u_z(\boldsymbol{x}^p(t), t)\rangle$ is significantly enhanced with increasing R_λ when $St \gtrsim 0.2$, whereas it is almost insensitive to R_λ when $St \lesssim 0.1$.

The results in figure 5 also show that when scales larger than some finite ℓ_F/η are filtered out, so that the range of scales contained in u_z' is the same for each R_λ, the R_λ dependence of $\langle u_z'(\boldsymbol{x}^p(t), t)\rangle$ is dramatically suppressed. Indeed, for $St \gtrsim 0.4$ the effect of R_λ is entirely suppressed for ℓ_F/η values considered. This confirms that the strong effect of R_λ on $\langle u_z(\boldsymbol{x}^p(t), t)\rangle$ is principally due to the enhanced range of scales available for the particles to preferentially sample as R_λ is increased. Recall that increasing R_λ leads to two distinct effects, namely an increased range of flow scales, and enhanced intermittency. While filtering eliminates the effect of the increased range of scales by removing scales greater than ℓ_F (so that each flow of differing R_λ has the same range of scales), the effect of enhanced intermittency still remains. It can be seen in figure 5 that for $\ell_F/\eta \leqslant 125.6$, the curves collapse for $St \gtrsim 0.4$, while there is a residual effect of R_λ for $St \lesssim 0.3$, which must be due to intermittency. That the effect of intermittency is only apparent for small St is consistent with previous works which show that the effect of flow intermittency on inertial particle motion in turbulence is mainly confined to small St, while larger St particles filter out the effects of intermittent fluctuations in the flow (Bec *et al.* 2006; Ayyalasomayajula, Warhaft & Collins 2008).

https://doi.org/10.1017/jfm.2019.337 Published online by Cambridge University Press

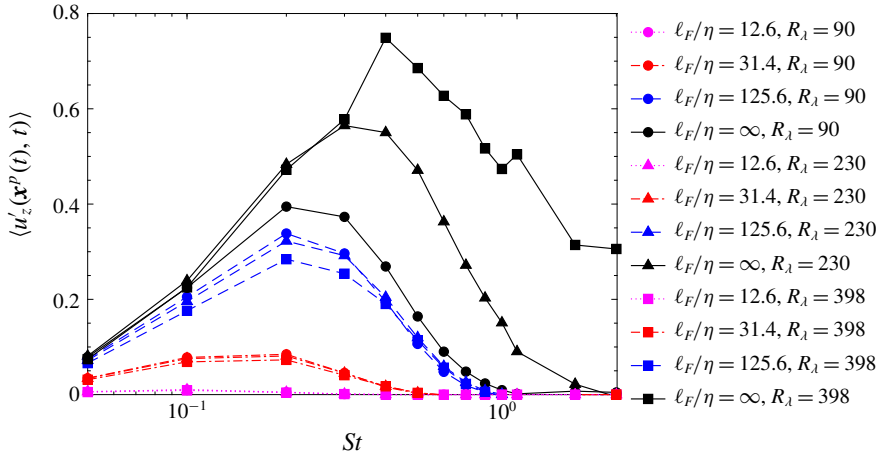


FIGURE 5. (Colour online) DNS results for $\langle u_z'(\boldsymbol{x}^p(t), t)\rangle$ as a function of St, for $Fr = 0.052$, and for various filtering lengths ℓ_F/η. The circles correspond to $R_\lambda = 90$, the triangles to $R_\lambda \approx 230$ and the squares to $R_\lambda = 398$. The solid lines correspond to $\ell_F/\eta = \infty$, the dashed lines to $\ell_F/\eta = 125.6$, the dash-dot lines to $\ell_F/\eta = 31.4$ and the dotted lines to $\ell_F/\eta = 12.6$.

To observe the effect of R_λ more clearly, in figure 6, we plot $\mathcal{A}(R_\lambda, St)/\mathcal{A}(R_\lambda = 90, St)$ where $\mathcal{A}(R_\lambda, St) \equiv \langle u_z(\boldsymbol{x}^p(t), t)\rangle/u_\eta$, as a function of R_λ and for different values of St. In agreement with the theoretical analysis, as St is increased, $\mathcal{A}(R_\lambda, St)/\mathcal{A}(R_\lambda = 90, St)$ becomes increasingly sensitive to R_λ. The analysis leads us to expect that for any St, the ratio $\mathcal{A}(R_\lambda, St)/\mathcal{A}(R_\lambda = 90, St)$ will eventually saturate at sufficiently large R_λ and the R_λ at which saturation occurs would increase with St. Our data are consistent with this, however, we do not have enough R_λ data points to be conclusive, and data at larger R_λ are required to observe the saturation for $St = O(1)$. Again, this is because in order to observe the saturation we must consider values of R_λ for which $\ell_c(St) < L(R_\lambda)$, and our DNS does not satisfy this for $R_\lambda \leqslant 398$ and $St = O(1)$.

4.3. *Influence of Froude number on the scales governing particle settling speeds*

Another prediction of the theory is that for a given St, as Fr is decreased, $\ell_c(St)$ increases meaning that larger scales become responsible for the behaviour of $\langle u_z(\boldsymbol{x}^p(t), t)\rangle$. In figure 7, we plot $\langle u_z'(\boldsymbol{x}^p(t), t)\rangle$ for $Fr = 0.3$ and $Fr = 0.052$, each at $R_\lambda \approx 230$. For $St \gtrsim 0.1$, the results confirm the prediction, since they show that $\langle u_z(\boldsymbol{x}^p(t), t)\rangle$ is more strongly affected by filtering as Fr is decreased, which is equivalent to saying that $\langle u_z(\boldsymbol{x}^p(t), t)\rangle$ is affected by increasingly larger scales as Fr is decreased.

To show this more clearly, in figure 8 we plot the ratio $\langle u_z'(\boldsymbol{x}^p(t), t)\rangle/\langle u_z(\boldsymbol{x}^p(t), t)\rangle$ as a function of ℓ_F/η, for different Fr, St and for $R_\lambda \approx 230$. The results show that as Fr is decreased, the ratio decreases for a given St and ℓ_F/η. This confirms the prediction of the theory as it indicates that as Fr is decreased, larger scales become responsible for the enhanced particle settling speeds due to turbulence. This could also explain the increased cluster size (determined by Voronoi tessellation) in the presence of gravity observed by Baker *et al.* (2017). In particular, as the particles settle faster due to gravity, the scales at which the clustering mechanisms (such as the preferential

https://doi.org/10.1017/jfm.2019.337 Published online by Cambridge University Press

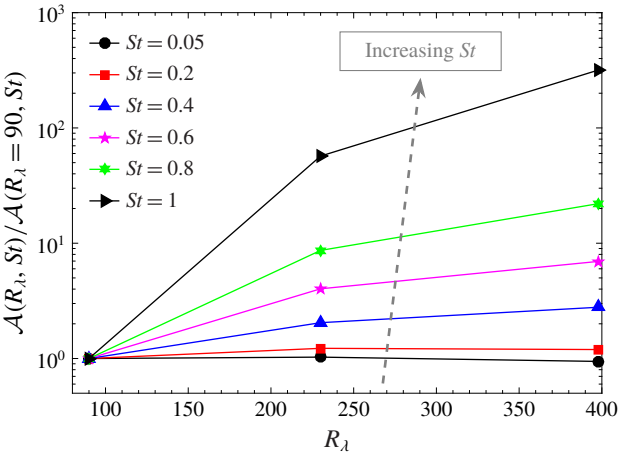


FIGURE 6. (Colour online) DNS results for $\mathcal{A}(R_\lambda, St)/\mathcal{A}(R_\lambda = 90, St)$ as a function of R_λ, for various St, and for $Fr = 0.052$.

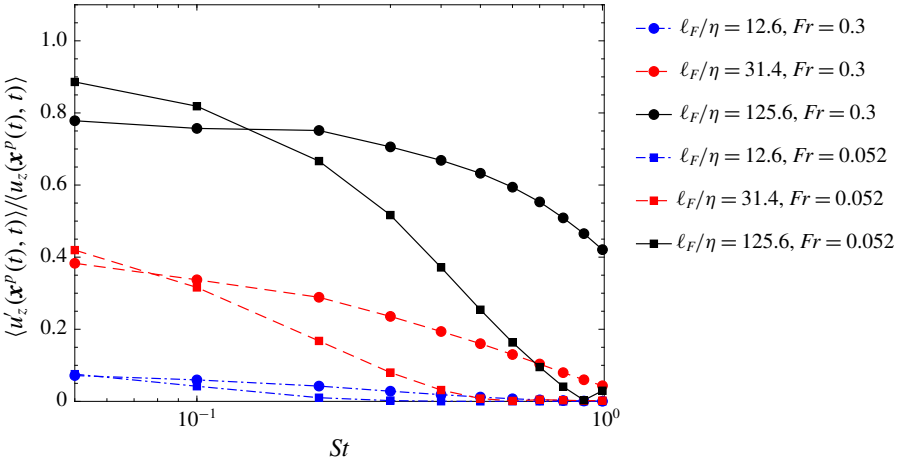


FIGURE 7. (Colour online) DNS results for $\langle u_z'(\boldsymbol{x}^p(t), t)\rangle/\langle u_z(\boldsymbol{x}^p(t), t)\rangle$ as a function of St for $Fr = 0.052$ (squares) and $Fr = 0.3$ (circles), and $R_\lambda \approx 230$. The solid lines correspond to $\ell_F/\eta = 125.6$, the dashed lines to $\ell_F/\eta = 31.4$, and the dash-dot lines to $\ell_F/\eta = 12.6$.

sampling of the filtered velocity gradient field, see Bragg *et al.* (2015)) become active move to larger scales.

4.4. *Scale dependence of preferential sweeping*

So far, we have tested the predictions following from our theoretical analysis regarding the scales that contribute to enhanced particles settling speeds in turbulence. We now turn to consider in more detail the multiscale nature of the preferential sweeping mechanism. Recall that the preferential sweeping mechanism involves the idea that the enhanced particle settling is associated with the tendency of inertial particles to preferentially sample the flow by preferring paths around the downward side of vortices. However, according to our theoretical analysis this preferential sweeping can

https://doi.org/10.1017/jfm.2019.337 Published online by Cambridge University Press

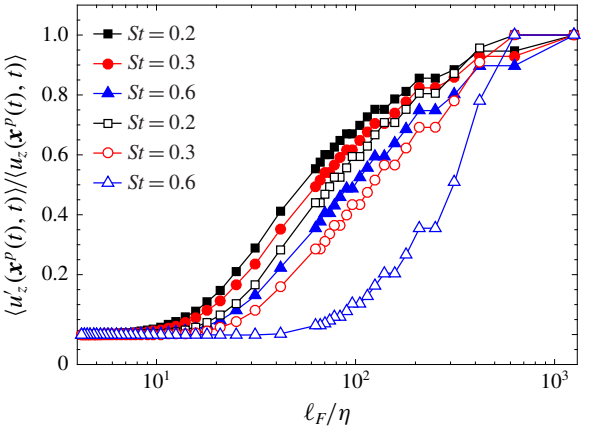


FIGURE 8. (Colour online) DNS data for $\langle u_z'(\boldsymbol{x}^p(t), t)\rangle/\langle u_z(\boldsymbol{x}^p(t), t)\rangle$ as a function of ℓ_F/η for different St, and $Fr = 0.3$ (filled symbols), $Fr = 0.052$ (open symbols), and $R_\lambda \approx 230$.

only take place at scales $\ell < \ell_c(St)$, such that the preferential sweeping mechanism is multiscale in general, and does not only involve the small scales as in the $St \ll 1$ analysis of Maxey (1987).

A traditional way to consider preferential sampling of the flow by inertial particles is to consider $\mathcal{Q}^p(t) \equiv \mathcal{S}^2(\boldsymbol{x}^p(t), t) - \mathcal{R}^2(\boldsymbol{x}^p(t), t)$, where $\mathcal{S}^2$ and $\mathcal{R}^2$ are the second invariants of the strain-rate $\boldsymbol{\mathcal{S}} \equiv (\boldsymbol{\nabla u} + \boldsymbol{\nabla u}^\top)/2$ and rotation-rate $\boldsymbol{\mathcal{R}} \equiv (\boldsymbol{\nabla u} - \boldsymbol{\nabla u}^\top)/2$ tensors, respectively. Comparing the statistics of $\mathcal{Q}^p(t)$ along fluid and inertial particle trajectories provides a clear way to consider preferential sampling since their statistics can only differ if the inertial particles are both non-uniformly distributed, and if their distribution is correlated to the local flow, i.e. if they exhibit preferential concentration. However, in order to consider how the particles preferential sample the flow at different scales we must instead consider the coarse-grained quantity $\widetilde{\mathcal{Q}}^p(t) \equiv \widetilde{\mathcal{S}}^2(\boldsymbol{x}^p(t), t) - \widetilde{\mathcal{R}}^2(\boldsymbol{x}^p(t), t)$, where $\widetilde{\mathcal{S}}^2 \equiv \widetilde{\boldsymbol{\mathcal{S}}} : \widetilde{\boldsymbol{\mathcal{S}}}$, $\widetilde{\mathcal{R}}^2 \equiv \widetilde{\boldsymbol{\mathcal{R}}} : \widetilde{\boldsymbol{\mathcal{R}}}$ and $\widetilde{\boldsymbol{\mathcal{S}}}$, $\widetilde{\boldsymbol{\mathcal{R}}}$ denote $\boldsymbol{\mathcal{S}}$, $\boldsymbol{\mathcal{R}}$ coarse grained on the scale ℓ_F.

In figure 9, we plot the PDF of $\widetilde{\mathcal{Q}}^p(t)$, namely

$$\mathcal{P}(\widetilde{\mathcal{Q}}, t) \equiv \langle \delta(\widetilde{\mathcal{Q}}^p(t) - \widetilde{\mathcal{Q}})\rangle, \tag{4.1}$$

where $\widetilde{\mathcal{Q}}$ is the sample-space variable. The results are shown for $R_\lambda = 398$, $Fr = \infty$ and $Fr = 0.052$, and for different St and ℓ_F/η. The results show, as expected, that the role of St is different at different scales, which is because the behaviour of $\mathcal{P}(\widetilde{\mathcal{Q}}, t)$ at any scale depends upon St_ℓ, not St. The results also show the strong effect of gravity on the preferential sampling, which is to suppress it. For example, in figure 9(*c*), corresponding to the no gravity case, we see that preferential sampling is strongest for $St = 1$. However, the results in in figure 9(*d*) show that when gravity is active, the preferential sampling for $St = 1$ is very weak. The suppression of preferential sampling due to gravity at any scale is because as Fr is decreased, the particles fall through the flow faster, which in turn reduces the interaction time between the particles and flow eddies, thereby causing the centrifuging mechanism to be less efficient. We emphasize, however, that this does not mean that their clustering is diminished by gravity. Indeed it has been shown using DNS that for $St \gtrsim 1$, clustering is actually enhanced by

https://doi.org/10.1017/jfm.2019.337 Published online by Cambridge University Press

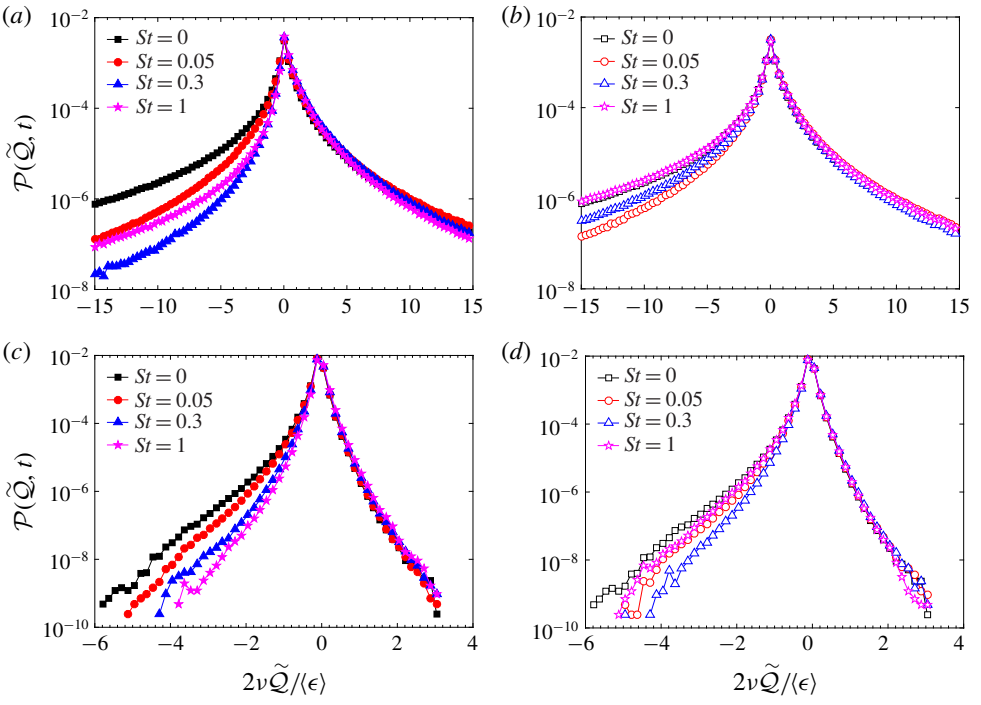


FIGURE 9. (Colour online) DNS data for $\mathcal{P}(\widetilde{\mathcal{Q}}, t)$ and different St. Panels (a,b) are for $\ell_F/\eta = 0$, while panels (c,d) are for $\ell_F/\eta = 66.1$. Panels (a,c) are for $Fr = \infty$, while panels (b,d) are for $Fr = 0.052$.

gravity (Bec *et al.* 2014; Ireland *et al.* 2016*b*). This is a reflection of the distinction between clustering and preferential concentration and the mechanisms responsible for each, as discussed in § 2.2. The subtle, but important point is that it is preferential concentration/sampling that determines the enhanced particle settling due to turbulence, and not clustering *per se* (see § 2.2).

Further quantitative information concerning the preferential sampling may be obtained by considering the quantity

$$\langle\widetilde{\mathcal{Q}}^p(t)\rangle/\sqrt{\langle[\widetilde{\mathcal{Q}}^p(t)]^2\rangle - \langle\widetilde{\mathcal{Q}}^p(t)\rangle^2}. \tag{4.2}$$

For homogeneous turbulence, this quantity is zero when measured along the trajectories of particles that do not preferentially sample the flow. The results in figure 10 show that with or without gravity, the maximum value for this quantity weakens as ℓ_F is increased. This then implies that the maximum preferential sampling decreases with increasing scale. As ℓ_F is increased, we also see that the peak value of the curve shifts to larger St. This can be explained by noting that we would expect the preferential sampling at any scale to be maximum for $St_\ell = O(1)$, and as ℓ is increased, the value of St for which $St_\ell = O(1)$ moves to larger St.

The results in figure 10 show that gravity significantly suppresses the preferential sampling at all scales, and the peak of the curves occurs at much lower St than in the no gravity case. This latter point can be understood by the fact that since the eddy

https://doi.org/10.1017/jfm.2019.337 Published online by Cambridge University Press

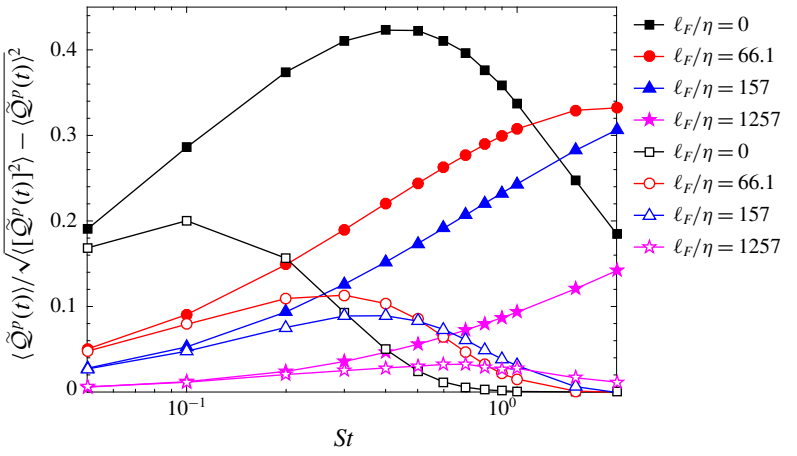


FIGURE 10. (Colour online) DNS data for $\langle\widetilde{\mathcal{Q}}^p(t)\rangle/\sqrt{\langle[\widetilde{\mathcal{Q}}^p(t)]^2\rangle-\langle\widetilde{\mathcal{Q}}^p(t)\rangle^2}$ as a function of St for different ℓ_F/η, for $Fr=\infty$ (filled symbols) and $Fr=0.052$ (open symbols), and $R_\lambda=398$.

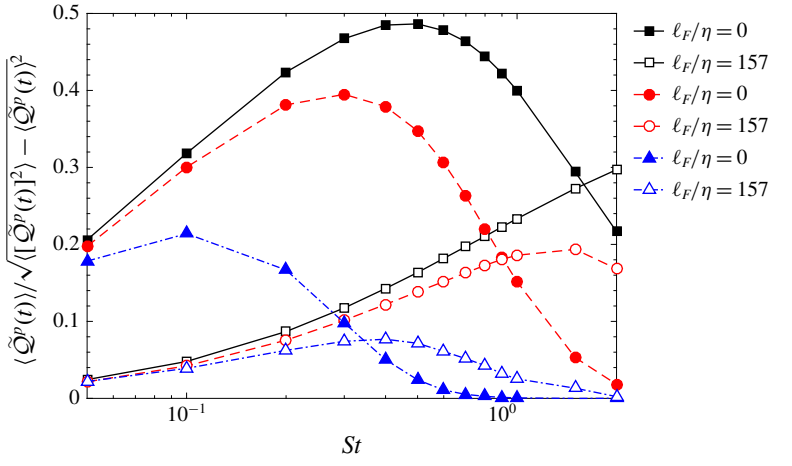


FIGURE 11. (Colour online) DNS data for $\langle\widetilde{\mathcal{Q}}^p(t)\rangle/\sqrt{\langle[\widetilde{\mathcal{Q}}^p(t)]^2\rangle-\langle\widetilde{\mathcal{Q}}^p(t)\rangle^2}$ as a function of St for $\ell_F/\eta=0$ (filled symbols) and $\ell_F/\eta=157$ (open symbols) at $R_\lambda\approx230$, and for $Fr=\infty$ (black solid lines), $Fr=0.3$ (red dashed lines), and $Fr=0.052$ (blue dash-dot lines).

turnover time scale seen by the particle T_ℓ decreases with decreasing Fr (for fixed St), then in order to observe $\tau_p/T_\ell=O(1)$ (at which one would expect the strongest preferential sampling) one has to go to smaller τ_p than in the case without gravity.

In figure 11, we show results corresponding to figure 10 but now for $R_\lambda\approx230$ and for three different values of Fr in order to further check the trends based on Fr observed in figure 10. The results confirm the trends observed in figure 10, showing that as Fr is decreased, the preferential sampling is systematically suppressed, and the St value at which the preferential sampling is strongest shifts to smaller values.

https://doi.org/10.1017/jfm.2019.337 Published online by Cambridge University Press

Finally, we pointed out earlier that results in Ireland *et al.* (2016*b*) showed that $\langle u_z(\boldsymbol{x}^p(t),t)\rangle > 0$ may be observed for $St \geqslant O(1)$ and $Fr \ll 1$, even though for $St \geqslant O(1)$ and $Fr \ll 1$ the particles do not preferentially sample the fluid velocity gradient field. The results in figures 10 and 11 for $\ell_F/\eta = 0$ indeed show that for $St \geqslant O(1)$ and $Fr = 0.052$, the particles do not preferentially sample the fluid velocity gradient field. Nevertheless, the results in figure 5 show that for the same St and Fr, $\langle u_z(\boldsymbol{x}^p(t),t)\rangle$ is significantly positive. However, the results in figures 10 and 11 for $\ell_F/\eta > 0$ resolve this issue because they show that while particles with $St \geqslant O(1)$ and $Fr = 0.052$ do not preferentially sample the fluid velocity gradient field, they do preferentially sample the coarse-grained fluid velocity gradient field, i.e. $\langle \widetilde{\mathcal{Q}}^p(t)\rangle / \sqrt{\langle [\widetilde{\mathcal{Q}}^p(t)]^2\rangle - \langle \widetilde{\mathcal{Q}}^p(t)\rangle^2}$ becomes finite for $St \geqslant O(1)$ and $Fr = 0.052$ as ℓ_F/η is increased. This confirms the picture presented by our theoretical analysis that as St is increased, the scales responsible for the enhanced particle settling via preferential sweeping become larger.

5. Conclusions

In this paper, we have considered the multiscale nature of the mechanism leading to the enhanced settling speeds of small, heavy particles in isotropic turbulence. The traditional explanation of Maxey (1987) is that enhanced particle settling in turbulence occurs because inertial particles preferentially sample the fluid velocity gradient field, exhibiting a tendency to be swept around the downward moving side of vortices. This mechanism is known as the preferential sweeping mechanism (Wang & Maxey 1993). However, recent results have raised questions about the completeness of this explanation. Moreover, there are several outstanding questions concerning the role of different turbulent flow scales on the enhanced settling, and the role of the Taylor Reynolds number R_λ. The theoretical work of Maxey (1987) is not able to answer these questions due to its restriction to particles with Stokes numbers $St \ll 1$.

To address these questions we have developed a new theoretical framework for analysing the problem that is valid for arbitrary St. The theory utilizes a decomposition of the ensemble averaging operator for the system that allows us to construct a result that involves a particle velocity field that is well defined for all St, unlike the particle velocity field of Maxey (1987) that is only valid for $St \ll 1$. Coarse-graining decompositions are also used in the theory in order to provide insight into the role of different scales in the turbulent flow on the particle settling speeds. Our theoretical result shows that the particle settling speeds are only affected by scales of the flow with size $\ell < \ell_c(St)$, where $\ell_c(St)$ is the length scale beyond which the effects of particle inertia are asymptotically small. Since $\ell_c(St)$ is a non-decreasing function of St, our theory shows that as St is increased, increasingly larger scales contribute to the enhanced particle settling due to the turbulence. In other words, the preferential sweeping mechanism operates on progressively larger scales as St is increased. Several new insights and predictions follow from our theoretical analysis, which were then tested using DNS data.

First, our theoretical analysis predicts that the range of scales contributing to the enhanced particle settling depends upon St, and that as a result, there can be no single turbulent flow scale that characterizes the enhanced settling. This is contrary to several previous experimental and numerical works that claim on the basis of their data that the enhanced settling speeds depend on the r.m.s. velocity of the turbulence u' (associated with the large scales of the flow). Therefore, even though previous studies have pointed to certain aspects of the multiscale nature of the problem (e.g. that the settling speeds depend on u' and τ_η), they concluded that the relevant

https://doi.org/10.1017/jfm.2019.337 Published online by Cambridge University Press

turbulent velocity scale determining the particle settling speed is the same for any St. However, according to our analysis, the fluid velocity scale of the turbulence that dominates the settling enhancement depend essentially on St. The DNS results confirmed this prediction, showing that as St is increased, progressively larger scales of the flow contribute to the enhanced settling. However, while it is true that only scales with size $\ell < \ell_c(St)$ contribute, our estimates show that $\ell_c(St)$ is larger than might be expected, such that even for $St = O(0.1)$, scales much larger than the Kolmogorov length scale η contribute to the enhanced settling.

Second, our theoretical analysis predicts that the settling velocity of the particle will only be influenced by R_λ when the integral length scale of the flow L, is smaller than $\ell_c(St)$. Once $L > \ell_c(St)$, the R_λ dependence saturates because the particles are not affected by the additional scales of the flow that are introduced by increasing R_λ. When $St \ll 1$, $\ell_c(St)$ is relatively small and so the particle settling speed should show a weak dependence on R_λ. However, when $St = O(1)$, $\ell_c(St)$ can be large enough for the particles to feel the effects of the additional flow scales introduced by increasing R_λ. Our DNS results confirmed this prediction, and also provided evidence consistent with the idea that for any St, the particle settling speeds become independent of R_λ for sufficiently large R_λ. Other DNS results also confirmed that the dominant effect of R_λ on the particle settling speeds is through the scale separation in the flow that increases with increasing R_λ, rather than effects of intermittency. However, we did observe evidence of effects of intermittency on the settling speeds for $St \lesssim 0.3$.

Third, our theoretical analysis predicts that for a given St and R_λ, as the Froude number Fr is decreased, $\ell_c(St)$ increases, such that the faster the particles settle, the larger the scales that contribute to their enhanced settling. This is essentially a consequence of the fact that settling reduces the correlation time scale of the flow seen by the particles. Our DNS results confirmed this picture except for $St \lesssim 0.1$, where the opposite behaviour was observed in some cases. We are unsure as to the explanation for this.

Finally, we used our DNS data to examine the preferential sampling of the flow by the particles at different scales. The preferential sampling of the flow is part of the preferential sweeping mechanism, and our analysis suggests that the preferential sampling of the flow should occur at different scales depending on St and Fr. To examine this we computed the statistics of the difference between the second invariants of the coarse grained (at scale ℓ_F) strain-rate and rotation-rate tensors evaluated at the positions of the inertial particles $\boldsymbol{x}^p(t)$. The results showed that the strongest preferential sampling at any scale ℓ_F is associated with increasingly larger St as ℓ_F is increased. Moreover, for a given St, there is an optimum range of scales where the preferential sampling is strongest. As Fr is decreased, the preferential sampling is suppressed, which is again due to the fact that settling reduces the correlation time scale of the flow seen by the particles, reducing the ability of local flow structures to modify the spatial distribution of the particles. When $St = O(1)$ and $Fr \ll 1$, the particles sample the fluid velocity gradient field uniformly, yet they exhibit enhanced settling speeds due to the turbulence. This observation, which appears to contradict the traditional preferential sweeping mechanism, is explained by our theory as being due to the fact that for $St = O(1)$ and $Fr \ll 1$, the scales at which the preferential sweeping mechanism operate do not lie in the dissipation range, but at larger scales. The DNS results confirm this since they show that while particles with $St = O(1)$ and $Fr \ll 1$ do not preferentially sample the fluid velocity gradient field, they do preferentially sample the fluid velocity gradient field coarse grained at scale ℓ_F outside the dissipation range.

https://doi.org/10.1017/jfm.2019.337 Published online by Cambridge University Press

Acknowledgements

The authors wish to thank M. Momenifar for providing some of the data used in this paper, as well as routines for producing some of the plots. This work used the Extreme Science and Engineering Discovery Environment (XSEDE), which is supported by National Science Foundation grant no. ACI-1548562 (Towns *et al.* 2014). Specifically, the Comet cluster was used under allocation CTS170009.

REFERENCES

ALISEDA, A., CARTELLIER, A., HAINAUX, F. & LASHERAS, J. C. 2002 Effect of preferential concentration on the settling velocity of heavy particles in homogeneous isotropic turbulence. *J. Fluid Mech.* **468**, 77–105.

AYYALASOMAYAJULA, S., WARHAFT, Z. & COLLINS, L. R. 2008 Modeling inertial particle acceleration statistics in isotropic turbulence. *Phys. Fluids* **20**, 094104.

BAKER, L., FRANKEL, A., MANI, A. & COLETTI, F. 2017 Coherent clusters of inertial particles in homogeneous turbulence. *J. Fluid Mech.* **833**, 364–398.

BATCHELOR, G. K. 1967 *An Introduction to Fluid Dynamics*. Cambridge University Press.

BEC, J., BIFERALE, L., BOFFETTA, G., CELANI, A., CENCINI, M., LANOTTE, A. S., MUSACCHIO, S. & TOSCHI, F. 2006 Acceleration statistics of heavy particles in turbulence. *J. Fluid Mech.* **550**, 349–358.

BEC, J., HOMANN, H. & RAY, S. S. 2014 Gravity-driven enhancement of heavy particle clustering in turbulent flow. *Phys. Rev. Lett.* **112**, 184501.

BRAGG, A. D. & COLLINS, L. R. 2014 New insights from comparing statistical theories for inertial particles in turbulence: I. Spatial distribution of particles. *New J. Phys.* **16**, 055013.

BRAGG, A., SWAILES, D. C. & SKARTLIEN, R. 2012*a* Drift-free kinetic equations for turbulent dispersion. *Phys. Rev.* E **86**, 056306.

BRAGG, A., SWAILES, D. C. & SKARTLIEN, R. 2012*b* Particle transport in a turbulent boundary layer: Non-local closures for particle dispersion tensors accounting for particle-wall interactions. *Phys. Fluids* **24**, 103304.

BRAGG, A. D., IRELAND, P. J. & COLLINS, L. R. 2015 Mechanisms for the clustering of inertial particles in the inertial range of isotropic turbulence. *Phys. Rev.* E **92**, 023029.

BRAGG, A. D., IRELAND, P. J. & COLLINS, L. R. 2015 On the relationship between the non-local clustering mechanism and preferential concentration. *J. Fluid Mech.* **780**, 327–343.

CHAN, C. C. & FUNG, J. C. H. 1999 The change in settling velocity of inertial particles in cellular flow. *Fluid Dyn. Res.* **25** (5), 257–273.

CLIFT, R., GRACE, J. R. & WEBER, M. E. 1978 *Bubbles, Drops, and Particles*. Academic Press.

ELGHOBASHI, S. E. & TRUESDELL, G. C. 1993 On the two-way interaction between homogeneous turbulence and dispersed particles. 1. Turbulence modification. *Phys. Fluids* A **5**, 1790–1801.

EYINK, G. L. & ALUIE, H. 2009 Localness of energy cascade in hydrodynamic turbulence. 1. Smooth coarse graining. *Phys. Fluids* **21** (11), 115107.

FORNARI, W., PICANO, F., SARDINA, G. & BRANDT, L. 2016 Reduced particle settling speed in turbulence. *J. Fluid Mech.* **808**, 153–167.

FUNG, J. C. H. 1993 Gravitational settling of particles and bubbles in homogeneous turbulence. *J. Geophys. Res.* **98**, 20287–20297.

FUNG, J. C. H. 1998 Effect of nonlinear drag on the settling velocity of particles in homogeneous isotropic turbulence. *J. Geophys. Res.: Oceans* **103** (C12), 27905–27917.

GOOD, G. H., IRELAND, P. J., BEWLEY, G. P., BODENSCHATZ, E., COLLINS, L. R. & WARHAFT, Z. 2014 Settling regimes of inertial particles in isotropic turbulence. *J. Fluid Mech.* **759**, R3.

GRABOWSKI, W. W. & WANG, L.-P. 2013 Growth of cloud droplets in a turbulent environment. *Annu. Rev. Fluid Mech.* **45**, 293–324.

GUSEVA, K., DAITCHE, A., FEUDEL, U. & TÉL, T. 2016 History effects in the sedimentation of light aerosols in turbulence: The case of marine snow. *Phys. Rev. Fluids* **1**, 074203.

https://doi.org/10.1017/jfm.2019.337 Published online by Cambridge University Press

GUSTAVSSON, K. & MEHLIG, B. 2011 Ergodic and non-ergodic clustering of inertial particles. *Eur. Phys. Lett.* **96**, 60012.

VAN HINSBERG, M. A. T., THIJE BOONKKAMP, J. H. M., TOSCHI, F. & CLERCX, H. J. H. 2012 On the efficiency and accuracy of interpolation methods for spectral codes. *SIAM J. Sci. Comput.* **34** (4), B479–B498.

HUCK, P. D., BATESON, C., VOLK, R., CARTELLIER, A., BOURGOIN, M. & ALISEDA, A. 2018 The role of collective effects on settling velocity enhancement for inertial particles in turbulence. *J. Fluid Mech.* **846**, 1059–1075.

IRELAND, P. J., BRAGG, A. D. & COLLINS, L. R. 2016*a* The effect of Reynolds number on inertial particle dynamics in isotropic turbulence. Part 1. Simulations without gravitational effects. *J. Fluid Mech.* **796**, 617–658.

IRELAND, P. J., BRAGG, A. D. & COLLINS, L. R. 2016*b* The effect of Reynolds number on inertial particle dynamics in isotropic turbulence. Part 2. Simulations with gravitational effects. *J. Fluid Mech.* **796**, 659–711.

IRELAND, P. J., VAITHIANATHAN, T., SUKHESWALLA, P. S., RAY, B. & COLLINS, L. R. 2013 Highly parallel particle-laden flow solver for turbulence research. *Comput. Fluids* **76**, 170–177.

KAWANISI, K. & SHIOZAKI, R. 2008 Turbulent effects on the settling velocity of suspended sediment. *J. Hydrol. Engng* **134**, 261–266.

KIORBOE, T. 1997 Small-scale turbulence, marine snow formation, and planktivorous feeding. *Sci. Mar.* **61** (Suppl. 1), 141–158.

MAXEY, M. R. 1987 The gravitational settling of aerosol particles in homogeneous turbulence and random flow fields. *J. Fluid Mech.* **174**, 441–465.

MAXEY, M. R. & CORRSIN, S. 1986 Gravitational settling of aerosol particles in randomly oriented cellular flow fields. *J. Aero. Sci.* **43**, 1112–1134.

MAXEY, M. R. & RILEY, J. J. 1983 Equation of motion for a small rigid sphere in a nonuniform flow. *Phys. Fluids* **26**, 883–889.

MEI, R. 1994 Effect of turbulence on the particle settling velocity in the nonlinear drag range. *Intl J. Multiphase Flow* **20**, 273–284.

MOMENIFAR, M., DHARIWAL, R. & BRAGG, A. D. 2018 The influence of Reynolds and Froude number on the motion of settling, bidisperse inertial particles in turbulence. arXiv e-prints arXiv:1808.01537.

MONCHAUX, R. & DEJOAN, A. 2017 Settling velocity and preferential concentration of heavy particles under two-way coupling effects in homogeneous turbulence. *Phys. Rev. Fluids* **2**, 104302.

NEMES, A., DASARI, T., HONG, J., GUALA, M. & COLETTI, F. 2017 Snowflakes in the atmospheric surface layer: observation of particle turbulence dynamics. *J. Fluid Mech.* **814**, 592–613.

NIELSEN, P. 1984 On the motion of suspended sand particles. *J. Geophys. Res.: Oceans* **89** (C1), 616–626.

NIELSEN, P. 1993 Turbulence effects on the settling of suspended particles. *J. Sedim. Petrol.* **63**, 835–838.

PAPANICOLAOU, A. (THANOS) N., ELHAKEEM, M., KRALLIS, G., PRAKASH, S. & EDINGER, J. 2008 Sediment transport modeling review – current and future developments. *J. Hydraul. Engng* **134** (1), 1–14.

PETERSEN, A. J., BAKER, L. & COLETTI, F. 2019 Experimental study of inertial particles clustering and settling in homogeneous turbulence. *J. Fluid Mech.* **864**, 925–970.

POPE, S. B. 2000 *Turbulent Flows*. Cambridge University Press.

REEKS, M. W. 1977 On the dispersion of small particles suspended in an isotropic turbulent fluid. *J. Fluid Mech.* **83**, 529–546.

RILEY, J. J. & LINDBORG, E. 2012 *Recent Progress in Stratified Turbulence*, pp. 269–317. Cambridge University Press.

ROSA, B., PARISHANI, H., AYALA, O. & WANG, L.-P. 2016 Settling velocity of small inertial particles in homogeneous isotropic turbulence from high-resolution DNS. *Intl J. Multiphase Flow* **83**, 217–231.

ROSA, B. & POZORSKI, J. 2017 Impact of subgrid fluid turbulence on inertial particles subject to gravity. *J. Turbul.* **18** (7), 634–652.

https://doi.org/10.1017/jfm.2019.337 Published online by Cambridge University Press

SCHNEBORN, P.-R. 1975 The interaction between a single particle and an oscillating fluid. *Intl J. Multiphase Flow* **2** (3), 307–317.

SHAW, R. A. 2003 Particle-turbulence interactions in atmospheric clouds. *Annu. Rev. Fluid Mech.* **35**, 183–227.

SQUIRES, K. D. & EATON, J. K. 1991 Preferential concentration of particles by turbulence. *Phys. Fluids* A **3**, 1169–1178.

SUNDARAM, S. & COLLINS, L. R. 1997 Collision statistics in an isotropic, particle-laden turbulent suspension I. Direct numerical simulations. *J. Fluid Mech.* **335**, 75–109.

TOWNS, J., COCKERILL, T., DAHAN, M., FOSTER, I., GAITHER, K., GRIMSHAW, A., HAZLEWOOD, V., LATHROP, S., LIFKA, D., PETERSON, G. D., ROSKIES, R., SCOTT, J. R. & WILKINS-DIEHR, N. 2014 Xsede: Accelerating scientific discovery. *Comput. Sci. Engng* **16** (5), 62–74.

TUNSTALL, E. B. & HOUGHTON, G. 1968 Retardation of falling spheres by hydrodynamic oscillations. *Chem. Engng Sci.* **23** (9), 1067–1081.

WANG, L. P. & MAXEY, M. R. 1993 Settling velocity and concentration distribution of heavy particles in homogeneous isotropic turbulence. *J. Fluid Mech.* **256**, 27–68.

WILKINSON, M. & MEHLIG, B. 2005 Caustics in turbulent aerosols. *Europhys. Lett.* **71**, 186–192.

YANG, C. Y. & LEI, U. 1998 The role of turbulent scales in the settling velocity of heavy particles in homogeneous isotropic turbulence. *J. Fluid Mech.* **20**, 179–205.

YANG, T. S. & SHY, S. S. 2003 The settling velocity of heavy particles in an aqueous near-isotropic turbulence. *Phys. Fluids* **15**, 868–880.

ZAICHIK, L. I. & ALIPCHENKOV, V. M. 2009 Statistical models for predicting pair dispersion and particle clustering in isotropic turbulence and their applications. *New J. Phys.* **11**, 103018.

https://doi.org/10.1017/jfm.2019.337 Published online by Cambridge University Press